

1 **Parameter regionalization of a monthly water balance model for**  
2 **the conterminous United States**

---

3 **A.R. Bock<sup>1</sup>, L.E. Hay<sup>2</sup>, G.J. McCabe<sup>2</sup>, S.L. Markstrom<sup>2</sup>, and R.D. Atkinson<sup>3</sup>**

4 <sup>1</sup> U.S. Geological Survey, Colorado Water Science Center, Denver Federal Center, P.O. Box  
5 25046, MS 415, Denver, Colorado, 80225, USA

6 <sup>2</sup> U.S. Geological Survey, National Research Program, Denver Federal Center, P.O. Box 25046,  
7 MS 413, Denver, Colorado, 80225, USA

8 <sup>3</sup> U.S. Environmental Protection Agency, Office of Water (4503-T), 1200 Pennsylvania Ave.,  
9 Washington, DC, 20004, USA

10  
11 Correspondence to: A. Bock (abock@usgs.gov)

25 **Abstract**

26 A parameter regionalization scheme to transfer parameter values from gaged to ungaged areas  
27 for a monthly water balance model (MWBM) was developed and tested for the conterminous  
28 United States (CONUS). The Fourier Amplitude Sensitivity Test, a global-sensitivity algorithm,  
29 was implemented on a MWBM to generate parameter sensitivities on a set of 109,951 hydrologic  
30 response units (HRUs) across the CONUS. The HRUs were grouped into 110 calibration  
31 regions based on similar parameter sensitivities. Subsequently, measured runoff from 1,575  
32 streamgages within the calibration regions were used to calibrate the MWBM parameters to  
33 produce parameter sets for each calibration region. Measured and simulated runoff at the 1,575  
34 streamgages showed good correspondence for the majority of the CONUS, with a median  
35 computed Nash-Sutcliffe Efficiency coefficient of 0.76 over all streamgages. These methods  
36 maximize the use of available runoff information, resulting in a calibrated CONUS-wide  
37 application of the MWBM suitable for providing estimates of water availability at the HRU  
38 resolution for both gaged and ungaged areas of the CONUS.

39

40

41

42

43

44

45

46

47

48 **1 Introduction**

49 The WaterSMART program (<http://water.usgs.gov/watercensus/WaterSMART.html>) was started  
50 by the United States (U.S.) Department of the Interior in February 2010. Under WaterSMART,  
51 the National Water Census (NWC) was proposed as one of the U.S. Geological Survey's (USGS)  
52 key research directions with a focus on developing new hydrologic tools and assessments. One  
53 of the major components of the NWC is to provide estimates of water availability at a sub-  
54 watershed resolution nationally (<http://water.usgs.gov/watercensus/streamflow.html>) with the  
55 goal of determining if (1) the Nation has enough freshwater to meet both human and ecological  
56 needs and (2) this water will be available to meet future needs. Streamflow measurements do not  
57 provide direct observations of water availability at every location of interest; approximately 72  
58 percent (%) of land within the conterminous U.S. is gaged, with approximately 13% of these  
59 gaged areas being unaffected by anthropogenic effects (Kiang et al., 2013). This creates the  
60 challenge of determining the best method to transfer information from gaged catchments to data-  
61 poor areas where results cannot be calibrated or evaluated with measured streamflow (Vogel,  
62 2006). This transfer of model parameter information from gaged to ungaged catchments is  
63 known as hydrologic regionalization (Bloschl and Sivapalan, 1995).

64 Many hydrologic regionalization methods have focused on developing measures of similarity  
65 between gaged and ungaged catchments using spatial proximity and physical characteristics.  
66 These methods are highly dependent on the complexity of the terrain and scale at which the  
67 relations are derived. Spatial proximity is considered the primary explanatory variable for  
68 hydrologic similarity (Sawicz et al., 2011) because of the first-order effects of climatic and  
69 topographic controls on hydrologic response. Close proximity, however, does not always result  
70 in hydrologic similarity (Vandewiele and Elias, 1995; Smakhtin, 2001; Ali et al., 2012).

71 Physical characteristics have been used as exploratory variables to develop a better  
72 understanding of the relation between model parameters that represent model function, and  
73 physical properties of the catchment (Merz and Bloschl, 2004). The relation between model  
74 parameters and the relevant physical characteristics, expressed for example as a form of  
75 multivariate regression, can be transferred to ungaged catchments (Merz and Bloschl, 2004).  
76 Model parameter definitions are by nature ambiguous and often difficult to correlate to a small

77 number of meaningful variables such as physical and climatic characteristics (Zhang et al.,  
78 2008); some studies have found no significant correlation between catchment attributes and  
79 model parameters (Seibert, 1999; Peel et al., 2000), whereas others found that high correlation  
80 does not guarantee parameters that result in reliable model simulations of measured data (Sefton  
81 and Howarth, 1998; Kokkonen et al., 2003; Oudin et al., 2010). Physical characteristics also are  
82 used to classify catchments into discrete regions or clusters based on similarity in multi-  
83 dimensional attribute space (Oudin et al, 2008, 2010; Samuel et al., 2011). While these methods  
84 have indicated some success in simulating behavior of specific hydrologic components, such as  
85 base flow (Santhi et al., 2008), other efforts utilizing discrete clusters performed poorly in  
86 explaining variability of measured streamflow (McManamay et al., 2011).

87 Two important components of the transfer of parameters to ungaged catchments are the  
88 identification of (1) influential (and non-influential) parameters, and (2) geographic extents and  
89 scales at which parameters exert control on model function. Reducing the number of parameters  
90 is important for calibration efficiency by reducing the structural bias of the model and the  
91 uncertainty of results where they cannot be verified or confirmed (Van Griensven et al., 2006). A  
92 high number of calibrated, poorly constrained parameters can often mask data or structural  
93 errors, which can go undetected and reduce the skill of the model in replicating results outside of  
94 calibration conditions (Kirchner, 2006; Blöschl et al., 2013). This increases the potential for  
95 equifinality of parameter sets and higher model uncertainty that can be propagated to model  
96 results (Troch et al., 2003).

97 Sensitivity analysis (SA) has advanced the understanding of parameter influence on model  
98 behavior and structural uncertainty. SA measures the response of model output to variability in  
99 model input and/or model parameter values. SA partitions the total variability in the model  
100 response to each individual model parameter (Reusser et al., 2011) and results in a more-defined  
101 set of parameters and parameter ranges. Identification of sensitive parameters and their ranges is  
102 important for hydrologic model applications as key model parameters can vary spatially across  
103 physiographic regions, and also temporally (Tang et al., 2007; Guse et al., 2013).

104 Until recently, the high computational demands of SA have limited most implementations of  
105 hydrologic model SA to local sensitivity algorithms that evaluate a single parameter at a time

106 (Tang et al., 2007). Global SA uses random or systematic sampling designs of the entire  
107 parameter space to quantify variation in model output (Van Griensven et al. 2006, Reusser et al.  
108 2011). Some of these methods can account for parameter interaction and quantify sensitivity in  
109 non-linear systems. Global SA methods are computationally intensive (Cuo et al., 2011), but  
110 ever increasing computational efficiency has allowed for the development and application of a  
111 large number of global SA algorithms.

112 Previous work has suggested that isolating the key parameters that control model performance  
113 can be used to infer dominant physical processes in the catchment, as well as which components  
114 of the model dominate hydrologic response (Van Griensven et al. 2006, Tang et al., 2007,  
115 Reusser et al., 2011). To date, there has been little analysis of the use of SA for deriving  
116 measures of hydrologic similarity across catchments that can be applied towards hydrologic  
117 regionalization of model parameters. The spatially-distributed application of SA could be used  
118 to provide additional information for the delineation of homogeneous regions for parameter  
119 transfer based on similarity of model results from the SA. This strategy allows for the use of the  
120 existing model information and configuration to develop a calibration and regionalization  
121 framework without significantly changing the model structure or implementation

122 In this study, we present a hydrologic regionalization methodology for the CONUS that derived  
123 regions of hydrologic similarity based on the response of a Monthly Water Balance Model  
124 (MWBM) to parameter SA. Groups of streamgages within each region are calibrated together to  
125 define a single parameter set for each region. By extending model calibration to a large number  
126 of sites grouped by similarity through a quantified measure of model behavior, a more specific  
127 and constrained parameter space that fits each region can be identified.

## 128 **2 Methods**

### 129 **2.1 Monthly Water Balance Model**

130 The MWBM (Fig. 1) is a modular accounting system that provides monthly estimates of  
131 components of the hydrologic cycle by using concepts of water supply and demand (Wolock and  
132 McCabe 1999; McCabe and Markstrom, 2007). Monthly temperature (T) is used to compute  
133 potential evapotranspiration (PET) and to partition monthly precipitation (P) into rain and snow

134 (Fig. 1). Precipitation that occurs as snow is accumulated in a snow pack (snow storage as snow  
135 water equivalent, or SWE); rainfall is used to compute direct runoff ( $R_{\text{direct}}$ ) or overland flow,  
136 actual evapotranspiration (AET), soil-moisture storage recharge, and surplus water, which  
137 eventually becomes runoff (R) (Fig. 1). When rainfall for a month is less than PET, AET is equal  
138 to the sum of rainfall, snowmelt, and the amount of moisture that can be removed from the soil.  
139 The fraction of soil-moisture storage that can be removed as AET decreases linearly with  
140 decreasing soil-moisture storage; that is, water becomes more difficult to remove from the soil as  
141 the soil becomes drier and less moisture is available for AET. When rainfall (and snowmelt)  
142 exceeds PET in a given month, AET is equal to PET; water in excess of PET replenishes soil-  
143 moisture storage. When soil-moisture storage reaches capacity during a given month, the excess  
144 water becomes surplus and a fraction of the surplus ( $R_{\text{surplus}}$ ) becomes R, while the remainder of  
145 the surplus is temporarily held in storage. The MWBM has been previously used to examine  
146 variability in runoff over the CONUS (Wolock and McCabe, 1999; Hay and McCabe 2002;  
147 McCabe and Wolock, 2011a) and the global extent (McCabe and Wolock, 2011b). Table 1 lists  
148 the MWBM parameters, with definitions and parameter ranges for calibration.

149 The  $Ppt_{adj}$  and  $Tav_{adj}$  parameters specify seasonal adjustments for precipitation and  
150 temperature, respectively. The seasonal adjustment parameters were included to account for  
151 errors in the precipitation and temperature data used in this analysis. Sources of systematic and  
152 non-systematic errors of climate forcing data are well documented from the precipitation gage-  
153 derived sources (Groisman and Legates, 1994; Adam and Lettenmaier, 2003). Interpolation of  
154 these systematic errors from point-scale to gridded domains may propagate these biases,  
155 especially in complex terrain (Clark and Slater, 2006; Oyster et al, 2015). The use of adjustment  
156 factors allows uncertainty associated with forcing data and model parameter values to be treated  
157 separately (Vrugt et al., 2008).

158 *Figure 1. Conceptual diagram of the Monthly Water Balance Model (McCabe and Markstrom*  
159 *2007). Processes influenced by model parameters used in Fourier Amplitude Sensitivity Test*  
160 *(FAST) those identified by green arrow and numbered 1-5 (Table 1).*

161 Table 1. Monthly Water Balance Model parameters and ranges.

162 The MWBM was applied to the CONUS with 109,951 hydrologic response units (HRUs) from  
163 the Geospatial Fabric (Viger and Bock, 2014), a national database of hydrologic features for  
164 national hydrologic modeling applications (Fig. 2). This HRU derivation is based on an  
165 aggregation of the NHDPlus dataset (<http://www.horizon-systems.com/nhdplus/>), an integrated  
166 suite of geospatial data that incorporates features from the National Hydrography Dataset  
167 (<http://nhd.usgs.gov/>), the National Elevation Dataset (<http://ned.usgs.gov/>), and the Watershed  
168 Boundary Dataset (<http://nhd.usgs.gov/wbd.html>). The sizes of the HRUs range from less than 1  
169 square kilometer ( $\text{km}^2$ ) up to 67,991  $\text{km}^2$ , with an average size of 74  $\text{km}^2$ .

170 Inputs to the MWBM by HRU are: (1) monthly P (millimeters), monthly mean T (degrees  
171 Celsius), (2) latitude of the site (decimal degrees), (3) soil moisture storage capacity  
172 (millimeters), and (4) monthly coefficients for the computation of PET (dimensionless).  
173 Monthly P and mean T were derived from the daily time step,  $1/8^\circ$  gridded meteorological data  
174 for the period of record from January 1949 through December 2011 (Maurer et al., 2002).  
175 Monthly P and T data were aggregated for each HRU using the USGS Geo Data Portal  
176 (<http://cida.usgs.gov/climate/gdp/>) (Blodgett et al., 2011). Latitude was computed from the  
177 centroid of each HRU. Soil moisture storage capacity was calculated using a 1  $\text{km}^2$  grid derived  
178 from the Soils Data for the Conterminous United States (STATSGO) (Wolock, 1997). The  
179 monthly PET coefficients were calculated by calibrating the Hamon PET values to Farnsworth et  
180 al. (1982) mean monthly free-water surface evapotranspiration. McCabe et al. (2015) describes  
181 these PET coefficient calculations in detail.

182 *Figure 2. Hydrologic Response Units of the Geospatial Fabric, differentiated by color, overlain*  
183 *by NHDPlus region boundaries (R01-R18).*

## 184 **2.2 Fourier Amplitude Sensitivity Test**

185 A parameter SA for the CONUS was conducted for the MWBM using the Fourier Amplitude  
186 Sensitivity Test (FAST) to identify areas of hydrologic similarity. FAST is a variance-based  
187 global sensitivity algorithm that estimates the contribution to model output variance explained by  
188 each parameter (Cukier et al. 1973, 1975; Saltelli et al. 2000). Advantages of using FAST over  
189 other SA methods are that FAST can calculate sensitivities in non-linear systems, and is

190 extremely computationally efficient. The seasonal adjustment factors were not incorporated into  
191 the FAST analysis. We viewed the seasonal adjustment factors as more related to the forcing  
192 data, and for this application only parameters associated with model structure were included  
193 (first five parameters in Table 1).

194 FAST transforms a model's multi-dimensional parameter space into a single dimension of  
195 mutually independent sine waves with varying frequencies for each parameter, while using the  
196 parameter ranges to define each wave's amplitude (Cuker et al. 1973, 1975; Reusser et al. 2011).  
197 This methodology creates an ensemble of parameter sets numbering from 1 to N, each of which  
198 is unique and non-correlated with the other sets. Parameter sets are derived using the  
199 corresponding y-values along each parameter's sine wave given a value on the x-axis. The  
200 model is executed for all parameter sets using identical climatic and geographic inputs for each  
201 simulation. The resulting series of model outputs are Fourier-transformed to a power spectrum  
202 of frequencies for each parameter. Parameter sensitivity is calculated as the sum of the powers  
203 of the output variance for each parameter, divided by the sum of the powers of all parameters  
204 (Total Variance). The parameter sensitivities are scaled so that the sensitivities for all  
205 parameters sum to 1. Thus, parameters that explain a large amount of variability in the model  
206 output have higher (i.e. closer to 1) parameter sensitivity values.

207 FAST was implemented with the MWBM using the 'fast' library in the statistical software R  
208 (Reusser, 2012; R Core Team, 2013). Parameter ranges used by FAST for generating wave  
209 amplitudes of parameter ensembles across the CONUS were based on table 1. The 'fast' R  
210 package pre-determines the minimal number of runs necessary to estimate the sensitivities for  
211 the given number of parameters (Cukier et al., 1973). For our application we generated an  
212 ensemble of 1000 parameter sets (as compared to the minimally suggested number of 71  
213 estimated by 'fast'). The use of the minimal number of parameter sets should be a consideration  
214 for more complex models, but the relative computational efficiency and parallelization of the  
215 MWBM allowed the model to be simulated with this larger number of parameter sets quickly to  
216 help ensure a robust parameter sensitivity analysis.

217 Many applications of SA in hydrologic modeling have evaluated parameter sensitivity for  
218 measured streamflow using performance-based measures such as bias, root mean squared error



219 (RMSE), and the Nash-Sutcliffe Efficiency (NSE) (Nash and Sutcliffe, 1970; Moriasi et al.,  
220 2007). In this study, parameter sensitivity is examined using two hydroclimatic indices that  
221 account for the magnitude and variability of both climatic input and model output: the (1) Runoff  
222 Ratio (RR), a ratio of simulated runoff to precipitation, and (2) Runoff Variability (RV) index,  
223 the standard deviation of simulated runoff to the standard deviation of precipitation  
224 (Sankarasubramanian and Vogel, 2003).

### 225 **3 Parameter regionalization procedure**

226 The following sections describe the workflow for the MWBM calibration and regionalization  
227 (illustrated in Figure 3). The MWBM parameter sensitivities from the FAST analysis were  
228 evaluated across the CONUS. The spatial patterns and magnitudes of parameter sensitivities  
229 were used to organize the 109,951 HRUs into hydrologically similar regions referred to in the  
230 paper as calibration regions. During the initial streamgauge selection, potential streamgages were  
231 identified for use in the grouped MWBM calibration. These selected streamgages then were  
232 individually calibrated. Using a number of selection criteria, a final set of calibration gages were  
233 derived within each calibration region. The grouped MWBM calibration produced an ‘optimal’  
234 set of MWBM parameters for each calibration region by evaluating simulated MWBM variables  
235 converted to Z-scores.

236 *Figure 3. Schematic flowchart of the parameter regionalization procedure described in Section*  
237 *3: Parameter sensitivities (3.1), Calibration Regions (3.2), Initial Streamgauge Selection*  
238 *(3.3), and Grouped streamgauge calibration (3.4).*

#### 239 **3.1 Parameter sensitivities**

240 The relative sensitivities derived from the FAST analysis using the RR and RV indices at each of  
241 the 109,951 HRUs across the CONUS were scaled so that the five MWBM parameter  
242 sensitivities derived for each HRU summed to 100 (Fig. 4). RR (Fig. 4a) is most sensitive to the  
243 parameter *Drofac* in regions where MWBM runoff is not dominated by snowmelt and orographic  
244 precipitation, such as arid and sub-tropical areas of the CONUS. MWBM parameters that  
245 control snowpack accumulation and melt (*Meltcoef*, *Tsnow*, and *Train*) are more important to the  
246 RR in the extensive mountain ranges in the Western CONUS, and northerly latitudes around the

247 Great Lakes and in the Eastern CONUS. The RR indicates the highest sensitivity to the *Rfactor*  
248 parameter in mountainous areas of the CONUS and areas of the West Coast, and moderate to  
249 high sensitivity in areas where the sensitivity of RR to *Drofac* is low. *Tsnow*, *Train*, and  
250 *Meltcoef* all share similar patterns across the CONUS. The spatial variability of the sensitivity of  
251 RR to *Meltcoef* indicates different physical mechanisms controlling *Meltcoef* parameter influence  
252 on RR in different areas of the CONUS. In the Western CONUS, the sensitivity of RR to  
253 *Meltcoef* is greatest in mountainous areas that accumulate and hold snowpack through the late  
254 spring, such as the Rocky Mountains, Cascade, and Sierra Nevada mountain ranges. In the  
255 Eastern and Midwestern CONUS, the sensitivity of RR to *Meltcoef* is greatest for HRUs with  
256 more northerly latitudes.

257 *Figure 4. Relative sensitivity of the (a) Rainfall Ratio (RR) and (b) Runoff Variability (RV)*  
258 *indices to Monthly Water Balance Model parameters.*

259 The spatial patterns of sensitivities of RV to the five MWBM parameters (Fig. 4b) show both  
260 similarities and deviations from the patterns shown in the RR maps. For the central part of the  
261 CONUS, the relative sensitivity for the parameter *Drofac* is high for both indices, and low for the  
262 parameter *Rfactor* for both indices. *Meltcoef*, *Tsnow*, and *Train* share the same relations between  
263 higher sensitivity and higher elevation (primarily in the western part of the CONUS), and higher  
264 sensitivity and more northerly latitude (primarily in the eastern half of the CONUS) for both  
265 indices. However, *Drofac* and *Rfactor* show distinctly different patterns of relative sensitivities  
266 for the eastern part of the CONUS for RV as compared to RR. The other three parameters  
267 follow the same general spatial patterns for RV as compared to RR, but with greater fine-scale  
268 spatial variation and patchiness. The differences between the spatial distributions of the  
269 sensitivities between the two indices highlight that applying SA to different model outputs can  
270 generate different levels of sensitivities for each parameter. In addition, the choice of objective  
271 function or model output for which to measure parameter sensitivity is important, as parameter  
272 sensitivities will differ depending on whether a user evaluating measures of magnitude, the  
273 variability of distribution, or timing (Krause et al., 2005; Kapangaziwiri et al, 2012).

274 Figure 5 illustrates the variability of parameter sensitivities between NHDPlus regions 08 (Lower  
275 Mississippi) and 14 (Upper Colorado) (see Fig. 2) for the RR and RV indices, and between the

276 RR and RV within a single region. The Lower Mississippi and Upper Colorado NHDPlus  
277 regions have a similar number of HRUs (4,449 and 3,879, respectively) and cover a similar area  
278 (26,285 and 29,357 km<sup>2</sup>, respectively). The Lower Mississippi region has homogenous  
279 topography, with humid, subtropical climate, while the Upper Colorado region has highly  
280 variable topography, and thus highly variable climatic controls on hydrologic processes. For the  
281 Lower Mississippi region only one parameter dominates modeled RV variance (*Rfactor*, Fig. 5a)  
282 and modeled RR variance (*Drofac*, Fig. 5c). In contrast, for the Upper Colorado River region  
283 several parameters influence RV variability (*Drofac*, *Rfactor* and *Meltcoef*, Fig. 5b) and RR  
284 variability (*Drofac* and *Meltcoef*, Fig. 5d). In the Lower Mississippi Region the amount of  
285 snowfall is negligible, so the three parameters that control snowfall and snowpack accumulation  
286 in the MWBM have a negligible effect on the volume and variability of simulated total runoff.  
287 The *Rfactor* parameter controls almost all of the variance for the RV in the Lower Mississippi  
288 region. In humid, sub-tropical hydroclimatic regimes of the CONUS, peak runoff is coincident  
289 with peak precipitation, which is significant because these periods are when the surplus runoff is  
290 greatest. In the Upper Colorado, peak runoff is not coincident with peak precipitation, and the  
291 MWBM snow parameters have more control in modulating the variability and timing of runoff in  
292 the higher elevation HRUs. The comparison of the parameter sensitivities for these two regions  
293 illustrates how variable parameter sensitivities differ by region (i.e. different climatic and  
294 physiographic regions) and components of model response (i.e. volume and variability).

295 *Figure 5. Parameter sensitivities of Runoff Variability (RV; a-b) and Runoff Ratio (RR; c-d)*  
296 *indices for Monthly Water Balance Model parameters in the Lower Mississippi (R08) and*  
297 *Upper Colorado (R14).*

### 298 **3.2. Calibration regions**

299 The spatial patterns and magnitudes of parameter sensitivities across the CONUS were used as a  
300 basis for organizing HRUs into hydrologically similar regions for parameter regionalization  
301 through MWBM calibration. This idea is rooted in the hypothesis that geographically proximate  
302 HRUs share similar forcings and conditions, and thus will behave similarly. This application  
303 uses similarity in SA results as a basis for organization, rather than similarity in physiographic

304 characteristics. The derived regions are subsequently used to simplify model calibration across  
305 the CONUS and provide a basis for the transfer and application of parameters to unengaged areas.

306 The parameter sensitivities derived from the RR were used to organize the HRUs into two  
307 independently-derived calibration regions; the first derived by identifying HRUs with unique  
308 combinations of the order of parameter sensitivities to the RR (highest parameter sensitivities to  
309 lowest, i.e. 1-*Drofac* (78%), 2-*Rfactor* (16%), 3-*Meltcoef* (5%), 4-*Tsnow* (1%), 5-*Train* (1%)),  
310 and the second classification based upon identifying HRUs with unique sets of parameters whose  
311 sensitivities exceeded a specified threshold of parameter sensitivity (i.e. only *Drofac*, *Rfactor*,  
312 *Meltcoef* using a 5% threshold in the first classification example). The purpose of the first  
313 classification was to delineate regions of similar model response or behavior based on the order  
314 of importance of the MWBM parameters to the RR for each HRU. This classification identified  
315 16 distinct regions of HRUS across the CONUS based on the order of the parameter sensitivities  
316 of the five parameters (derived using the RR index). Sizes of these regions ranged from 94 km<sup>2</sup>  
317 to almost 2 million km<sup>2</sup>. The second classification delineated regions with an identical set of the  
318 most important parameters to the RR based on parameters whose sensitivities exceeded a 5%  
319 threshold. This step identified 12 regions of HRUs with unique combinations of parameter  
320 sensitivities exceeding 5%. There has been progress in providing quantitative thresholds for the  
321 identification of sensitive and non-sensitive parameters for hydrologic modelers (Tang et al.,  
322 2007), but no definitive consensus yet exists. Therefore a 5% threshold was used based on visual  
323 delineation of major physiographic features such as mountain ranges across the CONUS. The  
324 sizes of this second group of regions ranged from 94 km<sup>2</sup> to more than 15 million km<sup>2</sup>. Maps of  
325 the two groupings of HRUS were intersected to create a total of 49 regions across the CONUS.  
326 NHDPlus region and sub-region boundaries, proximity, and significant topographic divides were  
327 used to further divide the groups into 159 geographically unique calibration regions across the  
328 CONUS. The lack of streamgages available in some regions, especially areas with arid and  
329 semi-arid climates, necessitated merging regions together. Calibration regions that contained  
330 less than 3 streamgages from the 8,410 gages present in the Geospatial Fabric (see section 3.3)  
331 were combined with the proximate and most similar group which shared the most similar  
332 parameter sensitivities (both order and magnitude), resulting in 110 calibration regions across  
333 the CONUS (Fig. 6). Within each region the FAST results for both the RR and RV indices were

334 used to determine which parameters to calibrate. Within each region, parameters with a median  
335 parameter sensitivity of 5% for the RR and RV among the region's HRUs were selected for  
336 group calibration. Parameters not shown as sensitive were kept at the default value for the  
337 group.

338 *Figure 6. Final 110 Monthly Water Balance Model calibration regions differentiated by colors.*  
339 *A subset of streamgages within each calibration region were calibrated in a group-wise*  
340 *fashion to produce a single optimized parameter set for the entire region (Fig. 3).*

### 341 **3.3 Initial streamgauge selection**

342 The initial set of streamgages used for testing in the MWBM calibration procedures was selected  
343 from 8,410 streamgages identified in the Geospatial Fabric (Fig. 7). The Geospatial Fabric  
344 includes reference and non-reference streamgages from the Geospatial Attributes of Gages for  
345 Evaluating Streamflow dataset (GAGES-II, Falcone et al., 2010). Of the 8,410 streamgages in  
346 the Geospatial Fabric, 1,864 were identified as having reference-quality data with at least 20  
347 years of record. These reference quality streamgages were judged to be largely free of human  
348 alterations to flow (Falcone et al., 2010). In the current study, reference quality was not  
349 considered in the initial streamgauge selection because the 20 years of record was considered too  
350 restrictive. Therefore a subset of the 8,410 streamgages was selected for initial testing in the  
351 MWBM calibration procedures based on the following criteria:

- 352 (1) Remove streamgages with less than 10 years of total measured streamflow (120 months)  
353 within the time period 1950 – 2010.
- 354 (2) Remove streamgages with a drainage area defined by the Geospatial Fabric that are not  
355 within 5% of the USGS National Water Information System (NWIS) reported drainage  
356 area (U.S. Geological Survey, 2014). This eliminated many of the streamgages with  
357 smaller drainage areas due to the resolution of the Geospatial Fabric.
- 358 (3) Remove streamgages that did not have at least 75% of its drainage area contained within  
359 a single calibration region.

360 These criteria resulted in 5,457 potential streamgages for testing in the MWBM calibration  
361 procedures (Fig. 7). Streamflow at these streamgages was aggregated and converted from daily  
362 (cubic feet/second) to a monthly runoff depth (mm) (streamflow per unit area).

363 *Figure 7. Streamgages tested in the study. GF notes geospatial fabric for national hydrologic*  
364 *modeling (Viger and Bock, 2014).*

### 365 **3.4 Monthly Water Balance Model calibration**

366 Two automated calibration procedures were implemented to produce an ‘optimal’ set of MWBM  
367 parameters for each calibration region. The first procedure, Individual Streamgage Calibration,  
368 calibrated each of the 5,457 streamgages individually. Results from the individual calibrations  
369 were used to further filter the streamgages within the second procedure, Grouped Streamgage  
370 Calibration, which calibrated selected streamgages together by calibration region.

#### 371 **3.4.1 Individual streamgage calibration**

372 The first calibration procedure was an automated process that individually calibrated each of the  
373 5,457 streamgages from the initial streamgage selection with measured streamflow (U.S.  
374 Geological Survey, 2014). Results from these individual streamgage calibrations quantified the  
375 ‘best’ performance of the MWBM at each gage, providing a ‘baseline’ measure for evaluation.

376 The Shuffled Complex Evolution (SCE) global-search optimization algorithm (Duan et al., 1993)  
377 has been frequently used as an optimization algorithm in hydrologic studies (Hay et al., 2006;  
378 Blasone et al. 2007; Arnold et al., 2012), including previous studies with the MWBM (Hay and  
379 McCabe, 2010). Further details can be found in Duan et al. (1993). SCE was used to maximize a  
380 combined objective function based on: (1) Nash-Sutcliffe Efficiency (NSE) coefficient using  
381 measured and simulated monthly runoff and (2) NSE using natural log-transformed measured  
382 and simulated runoff (logNSE), using the entire period of record for each streamgage. The NSE  
383 measures the predictive power of the MWBM in matching the magnitude and variability of the  
384 measured and simulated runoff (Nash and Sutcliffe, 1970). The NSE coefficient ranges from  $-\infty$   
385 to 1, with 1 indicating a perfect fit, and values less than 0 indicating that measured mean runoff  
386 is a better predictor than model simulations. The NSE has been shown to give more weight to  
387 the larger values in a time series (peak flows) at the expense of lower values (low flows)

388 (Legates and McCabe, 1999), so the logNSE was incorporated into the objective function to give  
389 weight to lowflow periods (Tekleab et al., 2011).

### 390 **3.4.2 Grouped streamgage calibration**

391 The second calibration procedure was an automated process that calibrated groups of  
392 streamgages together for each calibration region to derive a single set of MWBM parameters  
393 (Table 1) for each calibration region (Fig. 6). The NSE and logNSE values from the individual  
394 streamgage calibrations (described in the previous section) were used to identify streamgages  
395 that should not be used for grouped streamgage calibration. If the individual streamgage  
396 calibration was not ‘satisfactory’, then it was felt that it would not provide useful information for  
397 the grouped streamgage calibration procedure.

398 Satisfactory individual streamgage calibrations were identified with the following procedure:

- 399 (1) Eliminate all streamgages with NSE values  $< 0.3$ .
- 400 (2) If the number of remaining streamgages for a given calibration region is  $> 10$ , then  
401 eliminate all streamgages with NSE  $< 0.5$ .
- 402 (3) If the number of streamgages for a given calibration region is  $> 25$ , then eliminate all  
403 streamgages with  $NSE_{log} < 0$ .
- 404 (4) If the number of remaining streamgages for a calibration region is  $< 5$ , check to see if any  
405 of the eliminated streamgages were reference streamgages (as defined in Falcone et al, 2010),  
406 then add the reference streamgages back in if the NSE value  $> 0.0$ . Reference streamgages are  
407 USGS streamgages deemed to be largely free of anthropogenic impacts and flow modifications  
408 (Falcone et al., 2010; Kiang et al., 2013).

409 These criteria, while somewhat arbitrary, were chosen so that no calibration region had less than  
410 5 streamgages for the grouped streamgage calibration. Using the above criterion, of the 5,457  
411 streamgages individually calibrated, 3,125 remained as candidates for the grouped streamgage  
412 calibration procedure.

413 The grouped streamgauge calibration procedure used the SCE global-search optimization  
 414 algorithm with a multi-term objective function (Eq. 1). Measured and simulated values for  
 415 selected streamgages contained within a calibration region were scaled to Z-scores to remove  
 416 differences in magnitudes between streamgages (Eq. 2). The multi-term objective function  
 417 minimized the sum of the absolute differences between Z-scores from four measured and  
 418 simulated time series: mean monthly runoff (MMO, MMS), monthly runoff (MO, MS), annual  
 419 runoff (AO, AS) (U.S. Geological Survey, 2014), and monthly snow water equivalent (SO, SS))  
 420 for all selected streamgages within a given calibration region:

$$421 \quad \min \sum_{i=1}^n [3|MMO_i - MMS_i| + |MO_i - MS_i| + |AO_i - AS_i| + 0.5|SO_i - SS_i|] \quad (\text{Eq.1})$$

422

$$\text{where } \begin{cases} 0 & \text{if } 0.75 < SO_i - SS_i < 1.25 \\ |SO_i - SS_i| & \text{if } SS_i < SO_i^{0.75} \\ |SO_i - SS_i| & SS_i > SO_i^{1.25} \end{cases}$$

423 The measured and simulated Z-scores were calculated as:

$$424 \quad Z = (x-u)/\sigma \quad (\text{Eq. 2})$$

425 where x is the time-series value, u is the mean, and  $\sigma$  the standard deviation of the measured and  
 426 simulated variable.

427 ‘Measured’ SWE was determined for each HRU from the Snow Data Assimilation System  
 428 (SNODAS; National Operational Hydrologic Remote Sensing Center, 2004) and included a +/-  
 429 25% error bound. The unconstrained automated calibration (without a restriction on SWE) led to  
 430 unrealistic sources of snowmelt in the summer that enhanced the low-flow simulations. The 25%  
 431 error bound is arbitrary; calibrating to the actual SNODAS SWE values was found to be too  
 432 restrictive, but adding this error bound to the SWE values resulted in better overall runoff  
 433 simulations. The absolute difference of the simulated SWE Z-scores that were within +/- 25% of  
 434 the measured SWE Z-score were designated as 0. Otherwise, the absolute difference was  
 435 computed between the simulated SWE Z-score and either the upper or lower bounds (Eq. 1).

436 The grouped calibration procedure was run for all 110 calibration regions. For each calibration  
 437 region the seasonal adjustment parameters and the sensitive parameters (identified by the FAST



438 analysis -- section 3.1) were calibrated; parameters deemed not sensitive (parameter sensitivity <  
439 5% of total variance) were set to their default values (see Table 1). The entire period of the  
440 streamflow record for each streamgauge was split by alternating years. After calibration, mean  
441 monthly measured and simulated Z-scores for runoff at all selected streamgages within a  
442 calibration region were compared.

443 Figure 8 shows an example of the graphic used to evaluate the measured and simulated mean  
444 monthly Z-scores for 21 streamgages selected for the region located in the Tennessee River  
445 calibration region (part of NHDPlus Region R06 in Fig. 2); the orange, red, and black dots  
446 indicate calibration, evaluation, and the entire period of record, respectively. A tight grouping  
447 around the one-to-one line indicates good correspondence between measured and simulated Z-  
448 scores. Points closer to the upper right corner of each plot represent high-flow periods. Points  
449 closer to the lower left corner of the plot represent low-flow periods. Streamgages within a  
450 calibration region were assigned the same parameter values; therefore streamgages that plotted  
451 outside (two standard deviations) of the one-to-one line were considered to not be representative  
452 of the calibration region, and the calibration procedure for that calibration region was repeated  
453 without those streamgages.

454 *Figure 8. Measured versus simulated mean monthly Z-scores for the Tennessee River*  
455 *calibration region (see Fig. 10b for location). Orange is calibration, red is evaluation, and*  
456 *black is all years.*

457 The goal of the second calibration procedure was to find a single parameter set for each  
458 calibration region. Past applications of the MWBM (Wolock and McCabe, 1999, McCabe and  
459 Wolock, 2011a) used a single set of fixed MWBM parameters for the entire CONUS. Many of  
460 the streamgages included in the second calibration procedure could be affected by significant  
461 anthropogenic effects; the seasonal adjustment factors, calibrated at each individual streamgauge,  
462 could account for these effects and result in satisfactory NSE values. Streamgages that were  
463 removed due to poor performance in the second calibration were assumed to have anthropogenic  
464 effects not consistent with the streamgages that plotted along the one-to-one line. Poor  
465 performance may result because the MWBM fails to reliably simulate runoff for a watershed  
466 because of model limitations (i.e. not including all important hydrologic processes), but the

467 calibration regions are assumed to be homogeneous based on the FAST analysis. Therefore it is  
468 assumed that if some of the streamgages within a region have satisfactory results, then the  
469 MWBM is able to simulate runoff in that region.

## 470 **4 MWBM calibration region results**

### 471 **4.1 Individual streamgage calibration results**

472 The individual streamgage calibrations provided information regarding: (1) the potential  
473 suitability of a given streamgage for inclusion in a grouped calibration, and (2) a ‘baseline’  
474 measure for evaluation of the grouped calibration results. Reference and non-reference  
475 streamgages were considered in this application; if the runoff at a streamgage could not be  
476 calibrated individually to a ‘satisfactory’ level (based on criterion outlined in section 3.4.2), then  
477 it was felt that it would not provide useful information for the grouped streamgage calibration  
478 procedure. Figure 9 shows the NSE (Fig. 9a) and logNSE (Fig. 9b) coefficients from the  
479 individual streamgage calibrations for the CONUS. Scattered throughout the CONUS are NSE  
480 and logNSE values less than 0.0 (triangles in Fig. 9). These poor results are likely streamgages  
481 with poor streamflow records, either due to measurement error or anthropogenic effects (dams,  
482 water use, etc.).

483 *Figure 9. Individual streamgage calibration results: (a) Nash-Sutcliffe Efficiency (NSE)*  
484 *coefficient and (b) log of the NSE (logNSE).*

### 485 **4.2 Grouped streamgage calibration results**

#### 486 **4.2.1 Mean monthly z-scores**

487 Figure 10a shows a scatterplot of measured versus simulated mean monthly Z-scores for runoff,  
488 similar to Figure 8, but based on all available years (the black dots in Fig. 8) for all the final  
489 calibration streamgages (1,575 streamgages). Four regions are highlighted to illustrate the  
490 monthly variability in MWBM results across the CONUS (see Fig. 10b for locations). The four  
491 regions are: New England (67 streamgages, red); Tennessee River basin (21 streamgages,  
492 orange); Platte Headwaters (15 streamgages, blue); and Pacific Northwest (33 streamgages,  
493 green) (Fig. 10b).

494 *Figure 10. (a) Measured versus simulated mean monthly Z-scores for runoff at all streamgages*  
495 *and (b) location of highlighted streamgages for four calibration regions: New England (67*  
496 *streamgages, red); Tennessee River (21 streamgages, orange); Platte Headwaters (15*  
497 *streamgages, blue); and Pacific Northwest (33 streamgages, green).*

498 In Fig. 10a, three of the regions (New England, Tennessee River, and Pacific Northwest), show  
499 simulated Z-scores that correspond favorably to measured Z-scores for each of the twelve  
500 months, including periods of low and high runoff. These regions represent marine or humid  
501 climates with homogenous physio-climatic conditions and an even spatial distribution of  
502 streamgages, where models should be expected to perform well (see Fig. 9) There is a higher  
503 variability in model results for the high-flow months (May - June) for streamgages within the  
504 Platte Headwaters (Fig. 10a; blue dots) than for low-flow months. This variability may be  
505 related to factors controlling the magnitude and timing of snow melt runoff (Fig. 9).

506 For each calibration streamgage, a set of four months were identified that represent different  
507 parts of the measured mean monthly hydrograph (highest- and lowest- flow month and the two  
508 median-flow months). The measured and simulated mean monthly streamflow Z scores  
509 corresponding to the four months are plotted as cumulative frequencies (Fig. 11) to compare how  
510 well the simulated Z scores matched measured Z scores for different parts of the hydrograph  
511 over the entire set of calibration gages. For the highest-flow, there is an under-estimation of  
512 runoff, with the greatest divergence between the two distributions in the middle to lower half of  
513 the distribution (Fig. 11a). For the median-flow, the measured and simulated Z scores are well  
514 matched. For the 10 lowest-flow, simulated Z scores are greater than measured Z scores, with the  
515 greatest divergence between the two distributions in the middle to upper half of the distribution  
516 (Fig. 11c).

517 *Figure 11. Z-score cumulative frequency for (a) highest-, (b) median-, and (c) lowest-flow*  
518 *months.*

519 The median Z-score errors (simulated - measured) by region for the (a) highest-, (b) median-,  
520 and (c) lowest-flows are shown in Figure 12. The largest errors are for the highest-flows (Fig.  
521 12a). The MWBM simulations under-estimate the highest flows for much of the CONUS. The

522 errors for median-flows are fairly uniform and consistent across the CONUS (Fig. 12b), with a  
523 median error close to 0. For the lowest-flow months the MWBM over-estimates low flows for a  
524 large portion of the Midwest (Fig. 12c).

525 *Figure 12. Z-score error (simulated - measured) for (a) highest-, (b) median-, and (c) lowest-*  
526 *flow months.*

#### 527 **4.2.2 Nash-Sutcliffe efficiency**

528 Figure 13 compares the NSE from the individual streamgage calibrations (gageNSE) with the  
529 grouped calibrations (groupNSE) for all final streamgages used in the second calibration  
530 procedure. NSE values  $> 0.75$  (dashed line) and  $> 0.5$  (solid line) indicate very good and  
531 satisfactory results (Moriassi et al., 2007). Overall, most NSE values fall above the 0.5 NSE  
532 threshold of satisfactory performance (median of gageNSE and groupNSE = 0.76). The gageNSE  
533 values are used here as a ‘baseline’ for evaluation of the groupNSE results. The groupNSE  
534 values were not expected to be greater than the gageNSE values since (1) NSE was not used as  
535 an objective function in the grouped calibration, and (2) grouped calibrations found the ‘best’  
536 parameter set for a set of streamgages versus an individual streamgage. Figure 13 shows an equal  
537 distribution of NSE values around the one-to-one line, indicating that the grouped calibration  
538 provided additional information over the individual streamgage calibrations (cases where  
539 groupNSE are greater than gageNSE in Fig. 13). The difference between the gageNSE and  
540 groupNSE becomes larger as the NSE values decrease, reflecting the increasing uncertainty in  
541 the grouped calibrations in areas with lower gageNSE values.

542 *Figure 13. Nash Sutcliffe Efficiency from individual (gageNSE) and grouped (groupNSE)*  
543 *calibration. Calibration regions in New England (67 streamgages, red); Tennessee River*  
544 *(21 streamgages, orange); Platte Headwaters (15 streamgages, blue); and Pacific Northwest*  
545 *(33 streamgages, green) are highlighted (see Fig. 10b for location).*

546 Four regions are highlighted in Fig. 13 to illustrate the variability of NSE across the CONUS  
547 (see Fig. 10b for locations). The highlighted regions in New England (red), Tennessee River  
548 (orange), and Pacific Northwest (green), show good groupNSE and gageNSE results. Four of

549 the 15 streamgages in the Platte Headwaters (blue) have groupNSE values  $\leq 0.5$ . This is  
550 probably related to simulation error during the snowmelt period (May - June, Fig. 10a).

551 Figure 14 shows the median groupNSE by calibration region for the CONUS. The pattern is very  
552 similar to that shown for the individual streamgage calibration results in Fig. 9a and highlights  
553 the problem areas shown in Fig. 12.

554 *Figure 14. Median Nash Sutcliffe Efficiency (NSE) of streamgages used for calibration by*  
555 *calibration region.*

556

## 557 **5 Discussion**

558 This study presented a parameter regionalization procedure for calibration of the MWBM,  
559 resulting in an application that can be used for simulation of hydrologic variables for both gaged  
560 and ungaged areas in the CONUS. The regionalization procedure grouped HRUs on the basis of  
561 similar sensitivity to five model parameters. Parameter values and model uncertainty  
562 information within a group was then passed from gaged to ungaged areas within that group.

### 563 **5.1 Regionalized parameters**

564 Results from this study indicate that regionalized parameters can be used to produce satisfactory  
565 MWBM simulations in most parts of the CONUS (Fig. 13). Despite the differences between the  
566 individual streamgage calibration and grouped calibration, Figure 13 illustrates that the grouped  
567 calibration strategy, which focused only on sensitive parameters, can provide just as much  
568 information as the individual streamgage calibration with no constraints on the parameter  
569 optimization other than the default ranges. The MWBM is a simple hydrologic model as it has  
570 minimal parameters, which are conceptual in nature (not physically based). It may be that this  
571 type of model is best for regionalization when parameter sensitivity can be identified and HRU  
572 behavior can be classified by a small number of clearly defined spatial groups. More  
573 complicated models with many more interactive parameters may not respond as well to this  
574 simple type of regionalization; more parameters may lead to more parameter interaction and  
575 situations of equifinality which might confuse the analysis.

576 The adjustments of precipitation and temperature parameters for the individual streamgage  
577 calibrations accounted for local errors such as rain gage under catch of precipitation. In addition  
578 these climate adjustments also account for local anthropogenic effects on streamflow (e.g. dams,  
579 diversions) since streamgages were not screened for these effects prior to individual streamgage  
580 calibration. In the grouped streamgage calibrations, the same precipitation and temperature  
581 adjustments are applied at every streamgage within the calibration region, making these climate  
582 adjustments more of a regional adjustment and producing more of a 'reference' condition for  
583 each calibration region.

## 584 **5.2 Parameter sensitivities and dominant process**

585 The MWBM parameter sensitivities varied by hydroclimatic index (RR and RV) and across the  
586 CONUS (Fig. 3). The parameter sensitivity patterns give an indication of dominant hydrologic  
587 processes based on MWBM. The dominant process can be seasonal and MWBM performance  
588 may be enhanced by extending the use of SA along the temporal domain to identify and  
589 temporally vary the parameters that are seasonally important to the MWBM. For example, error  
590 in peak flow months is the primary cause for poor model performance in the Platte Headwaters  
591 (Fig. 9). For the Platte Headwaters, the final parameter set performed well for simulated Z-  
592 scores for the regionalized low- and median-flow conditions (Fig. 9a, July through April), but  
593 was not able to replicate measured mean monthly flows for May and June. In this case, the  
594 dominant processes controlling hydrologic behavior change with season and the parameters  
595 controlling the dominant response may have to change accordingly (Gupta et al., 2008; Reusser  
596 et al., 2011).

## 597 **5.3 Model accuracy**

598 The pattern of MWBM accuracies shown in Fig. 8 and 14 are similar to those shown by Newman  
599 et al. (2015; Fig. 5a) in which a daily time-step hydrologic model was calibrated for 671 basins  
600 across the CONUS. Our study and the Newman et al. (2015) study both indicate the same  
601 'problem areas' with the poorest performing basins generally being located in the high plains and  
602 desert southwest. Newman et al. (2015) attributed variation in model performance by region to

603 spatial variations in aridity and precipitation intermittency, contribution of snowmelt, and runoff  
604 seasonality.

605 The inferior MWBM results in the ‘problem areas’ can be attributed to multiple factors which  
606 likely include inadequate hydrologic process representation and errors in forcing data (e.g.  
607 climate data), and/or measured streamflow. Archfield et al. (2015) state that the performance of  
608 continental-domain hydrologic models is considerably constrained by inadequate model  
609 representation of dominant hydrologic processes. For example, the simplicity of the MWBM  
610 presents limitations on the representation of deeper groundwater reservoirs, gaining and losing  
611 stream reaches, simplistic AET, and the effects of surface processes (infiltration and overland  
612 flow) that need to be represented at finer time steps than monthly.

613 The dominant hydrologic processes in the ‘problem areas’ appear to be poorly represented at the  
614 daily (Newman et al., 2015) and monthly time steps. This may be due to inadequate forcing  
615 data, the quality of which ‘is paramount in hydrologic modeling efforts’ (Archfield et al., 2015)  
616 and/or the lack of ‘good’ reference streamflow data for calibration and evaluation. Both surely  
617 play a role and emphasize the need for incorporation of additional datasets so that calibration and  
618 evaluation of intermediate states in the hydrologic cycle are examined.

## 619 **6 Conclusions**

620 A parameter regionalization procedure was developed for the CONUS that transferred parameter  
621 values from gaged to ungaged areas for a MWBM. The FAST global-sensitivity algorithm was  
622 implemented on a MWBM to generate parameter sensitivities on a set of 109,951 HRUs across  
623 the CONUS. The parameter sensitivities were used to group the HRUs into 110 calibration  
624 regions. Streamgages within each calibration region were used to calibrate the MWBM  
625 parameters to produce a regionalized set of parameters for each calibration region. The  
626 regionalized MWBM parameter sets were used to simulate monthly runoff for the entire  
627 CONUS. Results from this study indicate that regionalized parameters can be used to produce  
628 satisfactory MWBM simulations in most parts of the CONUS.

629 The best MWBM results were achieved simulating low- and median-flows across the CONUS.  
630 The high-flow months generally showed lower skill levels than the low- and median-flow

631 months, especially for regions with dominant seasonal cycles. The lowest MWBM skill levels  
632 were found in the high plains and desert southwest and can be attributed to multiple factors  
633 which likely include inadequate hydrologic process representation and errors in forcing data  
634 and/or measured streamflow. Calibration and evaluation of intermediary fluxes and states in the  
635 MWBM through additional measured datasets may help to improve MWBM representations of  
636 these model states by helping to constrain parameterization to measured values.



637 **7 Acknowledgments**

638 This research was financially supported by the U.S. Department of Interior South Central  
639 Climate Science Center (<http://southcentralclimate.org/>), U.S. Environmental Protection Agency  
640 Office of Water, and the U.S. Geological Survey WaterSMART initiative. This paper is a  
641 product of discussions and activities that took place at the USGS John Wesley Powell Center for  
642 Analysis and Synthesis (<https://powellcenter.usgs.gov/>). Further project support was provided  
643 by the Jeff Falgout of the USGS Core Science Systems (CSS) Mission Area. Any use of trade,  
644 product, or firm names is for descriptive purposes only and does not imply endorsement by the  
645 U.S. Government.

646

647

648

649

650

651

652

653

654

655

656

657

658 **8 References**

- 659 Adam, J.C., and Lettenmaier, D.P.: Bias correction of global gridded precipitation for solid  
660 precipitation undercatch, *J. Geophys. Res.*, 108, 1-14, doi:10.1029/2002JD002499, 2003.
- 661 Ali, G., Tetzlaff, D., Soulsby, C., McDonnell, L.L., and Capell, R.: A comparison of similarity  
662 indices for catchment classification using a cross-regional dataset, *Adv. Water Resources*, 40,  
663 11-22, <http://dx.doi.org/10.1016/j.advwatres.2012.01.008>, 2012.
- 664 Archfield, S.A., Clark, M., Areheimer, B., Hay, L.E., McMillan, H., Kiang, J.E., Seibert, J.,  
665 Bock, A., Wagener, T., Farmer, W.H., Andressian, V., Attinger, S., Viglione, A., Knight, R.,  
666 Markstrom, S., and Over, T.: Improving the performance of hydrologic models across local to  
667 continental domains: A discussion of research needs, *Water Resour. Res.*, 2015, In review.
- 668 Arnold, J.G., Moriasi, D.N., Gassman, P.W., Abbaspour, K.C., White, M.J., Srinivasan, R.,  
669 Santhi, C., Harmel, R.D., van Griensven, A., Van Liew, M.W., Kannan, N., and Jha, M.K.:  
670 SWAT: Model Use, Calibration and Validation, *T. ASABE*, 55(4), 1491-1508, 2012.
- 671 Blasone, R.-S., Madsen, H., and Rosbjerg, D.: Parameter estimation in distributed hydrological  
672 modelling: comparison of global and local optimisation techniques, *Nord. Hydrol.*, 34,451-476,  
673 doi:10.2166/nh.2007.024, 2007.
- 674 Blodgett, D.L., Booth, N.L., Kunicki, T.C., Walker, J.L., and Viger, R.J.: Description and  
675 Testing of the Geo Data Portal: A Data Integration Framework and Web Processing Services for  
676 Environmental Science Collaboration. US Geological Survey, Open-File Report 2011-1157, 9  
677 pp., Middleton, WI, USA, 2011.
- 678 Blöschl, G., and Sivapalan, M.: Scale issues in hydrological modeling: a review, *Hydrol.*  
679 *Process.*, 9, 251-290, 1995.
- 680 Blöschl, G., Sivapalan, M., Wagener, T., Viglione, A., and Savenije, H (Eds.): *Runoff Prediction*  
681 *in Ungauged Basins: Synthesis across Processes, Places, and Scales*. Cambridge University  
682 Press, Cambridge, England, 2013.

683 Clark, M.P., and Slater, A.G.: Probabilistic Quantitative Precipitation Estimation in Complex  
684 Terrain, B. Am. Meterol. Soc., 7, 3-2, doi: <http://dx.doi.org/10.1175/JHM474.1>, 2006.

685 Cukier, R.I., Fortuin, C.M., Shuler, K.E., Petschek, A.G, and Schaibly, J.H: Study of sensitivity  
686 of coupled reaction systems to uncertainties in rate coefficients 1, J. Chem. Phys., 59(8), 3873-  
687 3878, 1973.

688 Cukier, R.I., Schiably, J.H., and Shuler, K.E: Study of sensitivity of coupled reaction systems to  
689 uncertainties in rate coefficients 3, J. Chem. Phys., 63(3), 1140-1149, 1975.

690 Cuo, L., Giambelluca, T.W., and Ziegler, A.D: Lumped parameter sensitivity analysis of a  
691 distributed hydrological model within tropical and temperate catchments, Hydrol. Process.,  
692 25(15), 2405-2421, doi:10.1002/hyp.8017, 2011.

693 Duan, Q., Gupta, V.K., and Sorooshian, S.: A shuffled complex evolution approach for effective  
694 and efficient optimization, J. Optimiz. Theory App., 76, 501-521, doi:10.1007/BF00939380,  
695 1993.

696 Falcone, J.A., Carlisle, D.M., Wolock, D.M., and Meador, M.R.: GAGES: A stream gage  
697 database for evaluating natural and altered flow conditions in the conterminous United States,  
698 Ecology, 91, p. 621, A data paper in Ecological Archives E091-045-D1, available at  
699 <http://esapubs.org/Archive/ecol/E091/045/metadata.htm> (last accessed 15 November 2012),  
700 2010.

701 Farnsworth, R.K., Thompson, E.S., and Peck, E.L.: Evaporation Atlas for the Contiguous 48  
702 United States, NOAA Technical Report NWS 33, 41 pp., National Oceanic and Atmospheric  
703 Administration, Washington, D.C., 1982.

704 Groisman, P.Y., and Legates, D.R.: The accuracy of United States precipitation data, Bull. Am.  
705 Meterol. Soc., 75(2), 215-227, doi:10.1029/1998JD200110, 1994.

706 Gupta, H.V., Wagener, T., Liu, Y.Q. "Reconciling theory with observations: Elements of  
707 diagnostic approach to model evaluation." Hydrologic Processes (2008): 22, 3802-3813.

708 Guse, B., Reusser, D.E., and Fohrer, N.: How to improve the representation of hydrological  
709 processes in SWAT for a lowland catchment - temporal analysis of parameter sensitivity and  
710 model performance, *Hydrol. Process.*, 28(4), 2561-2670, doi:10.1002/hyp.9777, 2013.

711 Hay, L.E., Leavesley, G.H., Clark, M.P., Markstrom, S.L., Viger, R.J., and Umemoto, M.: Step-  
712 wise multiple-objective calibration of a hydrologic model for a snowmelt-dominated basin, *J.*  
713 *Am. Water Resour. A.*, 42(4), 877-890, doi:10.1111/j.1752-1688.2006.tb04501.x, 2006.

714 Hay, L.E., and McCabe, G.J.: Spatial Variability in Water-Balance Model Performance in the  
715 Conterminous United States, *J. Am. Water Resour. Assoc.*, 38(3), 847-860, DOI:  
716 10.1111/j.1752-1688.2002.tb01001.x, 2002.

717 Hay, L.E., and McCabe, G.J.: Hydrologic effects of climate change in the Yukon River Basin,  
718 *Climate Change*, 100, 509-523, doi:10.1007/s10584-010-9805-x, 2010.

719 Kapangaziwiri, E., Hughes, D. A., and Wagener, T.: Constraining uncertainty in hydrological  
720 predictions for ungauged basins in southern Africa, *Hydrol. Sci. J.*, 57, 1000–1019, 5  
721 doi:10.1080/02626667.2012.690881, 2012.

722 Kiang, J.E., Stewart, D.W., Archfield, S.A., Osborne, E.B., and Eng, K.: A National Streamflow  
723 Network Gap Analysis. U.S. Geological Survey, Scientific Investigative Reports 2013-5013, 94  
724 pp., Reston, VA, USA, 2013.

725 Kirchner, J.W.: Getting the right answers for the right reasons: Linking measurements,  
726 analyses, and models to advance the science of hydrology, *J. Hydrol.*, 42, W03S04,  
727 doi:10.1029/2005WR004362, 2006.

728 Kokkonen, T.S., Jakeman, A.J., Young, P.C., and Koivusalo, H.J.: Predicting daily flows in  
729 ungauged catchments: model regionalization from catchment descriptors at the Coweeta  
730 Hydrologic Laboratory, North Carolina, *Hydrol. Process.*, 17, 2219-2238, doi:10.1002/hyp.1329,  
731 2003.

732 Krause, P., Doyle, D. P., and Bäse, F.: Comparison of different efficiency criteria for  
733 hydrological model assessment, *Adv. Geosci.*, 5, 89–97, doi:10.5194/adgeo-5-89-2005, 2005.

734 Legates, D.R., and McCabe, G.J.: Evaluating the use of “goodness-of-fit” Measures in  
735 hydrologic and hydroclimatic model validation, *Water Resour. Res.*, 35(1), 233-241,  
736 doi:10.1029/1998WR900018, 1999.

737 Maurer, E.P., Wood, A.W., Adam, J.C., Lettenmaier, D.P., and Nijssen, B.: A long-term  
738 hydrologically-based data set of land surface fluxes and states for the conterminous United  
739 States, *J. Climatol.*, 15, 3237-3251, [http://dx.doi.org/10.1175/1520-](http://dx.doi.org/10.1175/1520-0442(2002)015<3237:ALTHBD>2.0.CO;2)  
740 [0442\(2002\)015<3237:ALTHBD>2.0.CO;2](http://dx.doi.org/10.1175/1520-0442(2002)015<3237:ALTHBD>2.0.CO;2), 2002.

741 McCabe, G.J., Hay, L.E., Bock, A., Markstrom, S.L., and Atkinson, D.R.: Inter-annual and  
742 spatial variability of Hamon potential evapotranspiration model coefficients, *J. Hydrol.*, 521,  
743 389-394, doi:10.1016/j.jhydrol.2014.12.006, 2015.

744 McCabe, G.J., and Markstrom, S.L.: A Monthly Water-Balance Model Driven By a Graphical  
745 User Interface. U.S. Geological Survey Open-File Report 2007-1008, 12 pp., Reston, VA, USA,  
746 2007.

747 McCabe, G.J., and Wolock, D.M.: Century-scale variability in global annual runoff examined  
748 using a water balance model, *Int. J. Climatol.*, 31, 1739-1748, doi:10.1002/joc.2198, 2011a.

749 McCabe, G.J., and Wolock, D.M.: Independent effects of temperature and precipitation on  
750 modeled runoff in the conterminous United States, *Water Resour. Res.*, 47, W1152,  
751 doi:10.1029/2011WR010630, 2011b.

752 McManamay, R.A., Orth, D.J., Dolloff, C.A., and Frimpong, E.A: Regional Frameworks  
753 applied to Hydrology: Can Landsapes-based frameworks capture the hydrologic variability?,  
754 *River Res. App.*, 28, 1325-1339, doi:10.1002/rra.1535, 2011.

755 Merz, R., and Bloschl, G.: Regionalisation of catchment model parameters, *J. Hydrol.*, 287, 95-  
756 123, doi:10.1016/j.jhydrol.2003.09.028, 2004.

757 Moriasi, D.N, Arnold, J.G., Van Liew, M.W., Bingner, R.L., Harmel, R.D., and Vieth, T.L.:  
758 Model Evaluation Guidelines for Systematic Quantification of Accuracy in Watershed  
759 Simulations, *T. ASABE*, 50, 885-900, 2007.

760 Nash, J.E., and Sutcliffe, J.V.: River flow forecasting through conceptual models Part I: a  
761 discussion of principles, *J. Hydrol.*, 10, 282-290, doi:10.1016/0022-1694(70)90255-6, 1970.

762 National Operational Hydrologic Remote Sensing Center, Snow data Assimilation System  
763 (SNODAS) Data Products at the NSIDC, 9/30/2003 through 6/13/2014, National Snow and Ice  
764 Data Center, Boulder, Colorado, USA, <http://dx.doi.org/10.7265/N5TB14TC>, 2004.

765 Newman, A.J., Clark, M.P., Sampson, K., Wood, A., Hay, L.E., Bock, A., Viger, R.J., Blodgett,  
766 D., Brekke, L., Arnold, J.R., Hopson, T., and Duan, Q.: Development of a large-sample  
767 watershed-scale hydrometeorological data set for the contiguous USA: data set characteristics  
768 and assessment of regional variability in hydrologic model performance, *Hydrol. Earth Syst. Sc.*,  
769 19, 209-223, doi:10.5194/hess-19-209-2015, 2015.

770 Oudin, L., Andreassian, V., Perrin, C., Michel, C., and Le Moine, N.: Spatial proximity,  
771 physical similarity, regression and ungauged catchments: a comparison of regionalization  
772 approaches based on 913 French catchments, *Water Resour. Res.*, 44, 1-15,  
773 doi:10.1029/2007WR006240, 2008.

774 Oudin, L., Kay, A., Andreassian, V., and Perrin, C.: Are seemingly physically similar  
775 catchments truly hydrologically similar?, *Water Resour. Res.*, 46, W11558,  
776 doi:10.1029/2009WR008887, 2010.

777 Oyler, J.W., Dobrowski, S.Z., Ballantyne, A.P., Klene, A.E., and Running, S.W.: Artificial  
778 amplification of warming trends across the mountains of the western United States, *Geophys.*  
779 *Res. Lett.*, 42, 153-161, doi:10.1002/2014GL062803, 2015.

780 Peel, M.C., Chiew, F.H.S., Western, A.W., and McMahon, T.A.: Extension of unimpaired  
781 monthly streamflow data and regionalization of parameter values to estimate streamflow in  
782 ungauged catchments. Report to National Land and Water Resources Audit, Center for  
783 Environmental Application and Hydrology, University of Melbourne, Parkville, 2000.

784 R Core Team: R: A language and environment for statistical computing, R Foundation for  
785 Statistical Computing, Vienna, Austria, 2013.

786 Reusser, D.: fast: Implementation of the Fourier Amplitude Sensitivity Test (FAST), R package  
787 version, <http://CRAN.R-project.org/package=fast>, (last access: 9 April 2014), 2012.

788 Reusser, D., Buytaert, W., and Zehe, E.: Temporal dynamics of model parameter sensitivity for  
789 computationally expensive models with the Fourier amplitude sensitivity test, *Water Resour.*  
790 *Res.*, 47, W07551, doi:10.1029/2010WR009947, 2011.

791 Saltelli, A., Tarantola, S., and Campolongo, F.: Sensitivity analysis as an ingredient of  
792 modeling, *Stat. Sci.*, 15, 377-395, 2000.

793 Samuel, J., Coulibaly, P., and Metcalfe, R.A.: Estimation of Continuous Streamflow in Ontario  
794 Ungauged Basins: Comparison of Regionalization Methods, *J. Hydrol. Eng.*, 16, 447-459,  
795 [http://dx.doi.org/10.1061/\(ASCE\)HE.1943-5584.0000338](http://dx.doi.org/10.1061/(ASCE)HE.1943-5584.0000338), 2011.

796 Sankarasubramanian, A., and Vogel, R.M.: Hydroclimatology of the continental United States,  
797 *Geophys. Res. Lett.*, 30, 1-4, doi:10.1029/2002GL015937, 2003.

798 Santhi, C., Kannan, N., Arnold, J.G., and Luzio, D.: Spatial calibration and temporal validation  
799 of flow for regional scale hydrologic modeling, *J. Am. Water Resour. Assoc.*, 4, 829-846,  
800 doi:10.1111/j.1752-1688.2008.00207.x, 2008.

801 Sawicz, K., Wagener, T., Sivapalan, M., Troch, P.A., and Carrillo, G.: Catchment classification:  
802 empirical analysis of hydrologic similarity based on catchment function in the eastern USA,  
803 *Hydrol. Earth Syst. Sc.*, 15, 2895-2911, 2011.

804 Sefton, C.E.M., and Howarth, S.M.: Relationships between dynamic response characteristics  
805 and physical descriptors of catchments in England and Wales, *J. Hydrol.*, 211, 11-16,  
806 doi:10.1016/S0022-1694(98)00163-2, 1998.

807 Seibert, J.: Regionalization of parameters for a conceptual rainfall runoff model, *Agr. Forest*  
808 *Meteorol.*, 98-99, 279-293, doi:10.1016/S0168-1923(99)00105-7, 1999.

809 Smakhtin, V.Y.: Low flow hydrology: a review, *J. Hydrol.*, 240, 147-186, doi:10.1016/S0022-  
810 1694(00)00340-1, 2001.

811 Tang, Y., Reed, P., Wagener, T., and van Werkhoven, T.: Comparing sensitivity analysis  
812 methods to advance lumped watershed model identification and evaluation, *Hydrol. Earth Syst.*  
813 *Sc.*, 11, 793-817, 2007.

814 Tekleab, S., Uhlenbrook, S., Mohamed, Y., Savenije, H.H.G., Temesgen, M., and Wenninger, J.:  
815 Water balance modeling of Upper Blue Nile catchments using a top-down approach, *Hydrol.*  
816 *Earth Syst. Sci.*, 15, 2179-2193, doi:10.5194/hess-15-2179-2011, 2011.

817 Troch, P.A., Paniconi, C., and McLaughlin, D.: Catchment-scale hydrological modeling and  
818 data assimilation, *Adv. Water Resour.*, 26, 131-135, doi:10.1016/S0309-1708(02)00087-8, 2003.

819 US Geological Survey: A National Water Information System, available at: <http://waterdata.usgs.gov/nwis/>  
820 (last access 27 March 2014), 2014.

821 Van Griensven, A., Meixner, T., Grunwald, S., Bishop, T., Diluzio, and M., Srinivasan, R.: A  
822 global sensitivity analysis tool for the parameters of multi-variable catchment models, *J. Hydrol.*,  
823 324, 10-23, doi:10.1016/j.jhydrol.2005.09.008, 2006.

824 Vandewiele, G.L., and Elias, A.: Monthly water balance of ungaged catchments obtained by  
825 geographical regionalization, *J. Hydrol.*, 170, 277-291, doi:10.1016/0022-1694(95)02681-E,  
826 1995.

827 Viger, R., Bock, A.: GIS Features of the Geospatial Fabric for National Hydrologic Modeling,  
828 U.S. Geological Survey, Denver, CO, USA, doi:10.5066/F7542KMD, 2014.

829 Vogel, R.M.: Regional calibration of watershed models, *Watershed Models*, Singh, V.P., and  
830 Frevert, D.F. (Eds.), CRC Press, Boca Raton, FL, USA, 2006.

831 Vrugt, J.A., ter Braak, C.J.F., Clark, M.P., Hyman, J.M., Robinson, B.A.: Treatment of input  
832 uncertainty in hydrologic modeling: Doing hydrology backwards with Markov Chain Monte  
833 Carlo simulation, *Water Resour. Res.*, 44, W00B09, doi:10.1029/2007WR006720, 2008.



834 Wolock, D.M.: STATSGO soil characteristics for the conterminous United States. U.S.  
835 Geological Survey Open-File Report 1997-656, Reston, VA, USA, available at:  
836 <http://water.usgs.gov/GIS/metadata/usgswrd/XML/muid.xml>, (last access 3 March 2012), 1997.

837 Wolock, D.M., and McCabe, G.J.: Explaining spatial variability in mean annual runoff in the  
838 conterminous United States, *Clim. Res.*, 11, 149-159, doi:10.3354/cr011149, 1999.

839 Zhang, X., Srinivasan, R., and Van Liew, M.: Multi-Site Calibration of the SWAT Model for  
840 Hydrologic Modeling, *T. ASABE*, 51, 2039-2049, 2008.

841

842

843

844

845

846

847

848

849

850

851

852

853

854

<b>Parameter</b>	<b>Definition</b>	<b>Range</b>	<b>Default</b>
<b>1. <i>Drofac</i></b>	Controls fraction of precipitation that becomes runoff	0, 0.10	0.05
<b>2. <i>Rfactor</i></b>	Controls fraction of surplus that becomes runoff	0.10, 1.0	0.5
<b>3. <i>Tsnow</i></b>	Threshold above which all precipitation is rain (°C)	-10.0, -2.0	-4.0
<b>4. <i>Train</i></b>	Threshold below which all precipitation is snow (°C)	0.0, 10.0	7.0
<b>5. <i>Meltcoef</i></b>	Proportion of snowpack that becomes runoff	0.0, 1.0	0.47
<b>6. <i>Ppt_adj</i></b>	Seasonal adjustment factor for precipitation (%)	0.5, 2.0	1
<b>7. <i>Tav_adj</i></b>	Seasonal adjustment for temperature (°C)	-3.0,3.0	0

855

856

Table 1. Monthly Water Balance Model parameters and ranges.

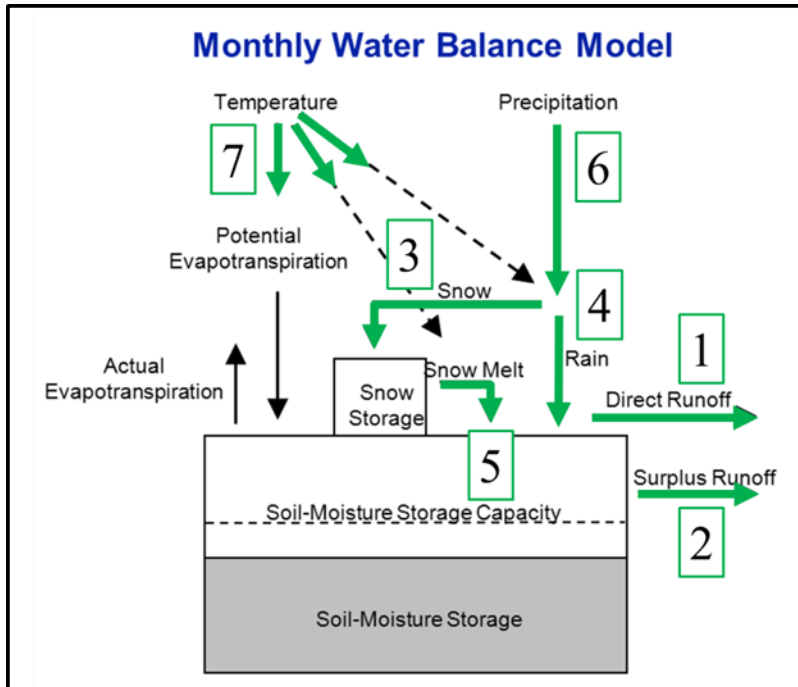
857

858

859

860

861



862

863 Figure 1. Conceptual diagram of the Monthly Water Balance Model (McCabe and Markstrom  
 864 2007). Processes influenced by model parameters used in Fourier Amplitude Sensitivity Test  
 865 (FAST) those identified by green arrow and numbered 1-5 (Table 1).

866

867

868

869

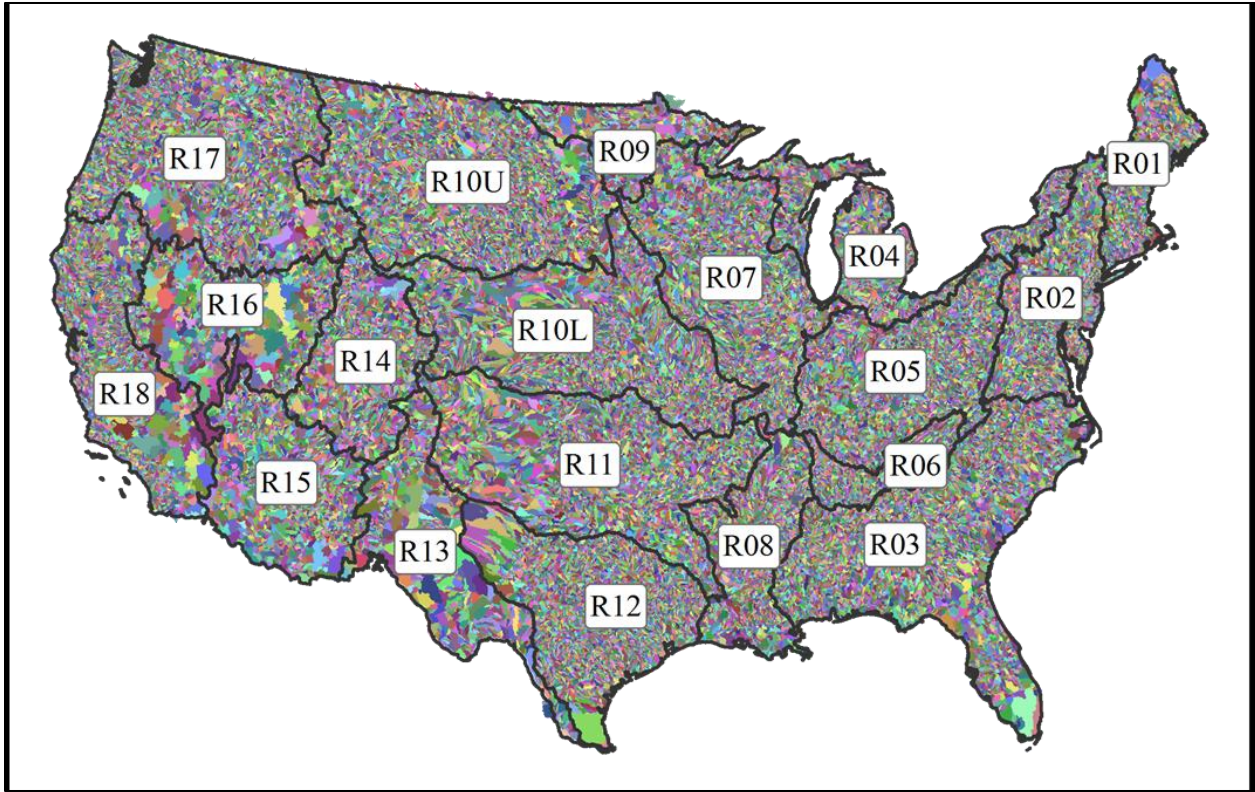
870

871

872

873

874



875

876 Figure 2. Hydrologic Response Units of the Geospatial Fabric, differentiated by color, overlain  
877 by NHDPlus region boundaries (R01-R18).

878

879

880

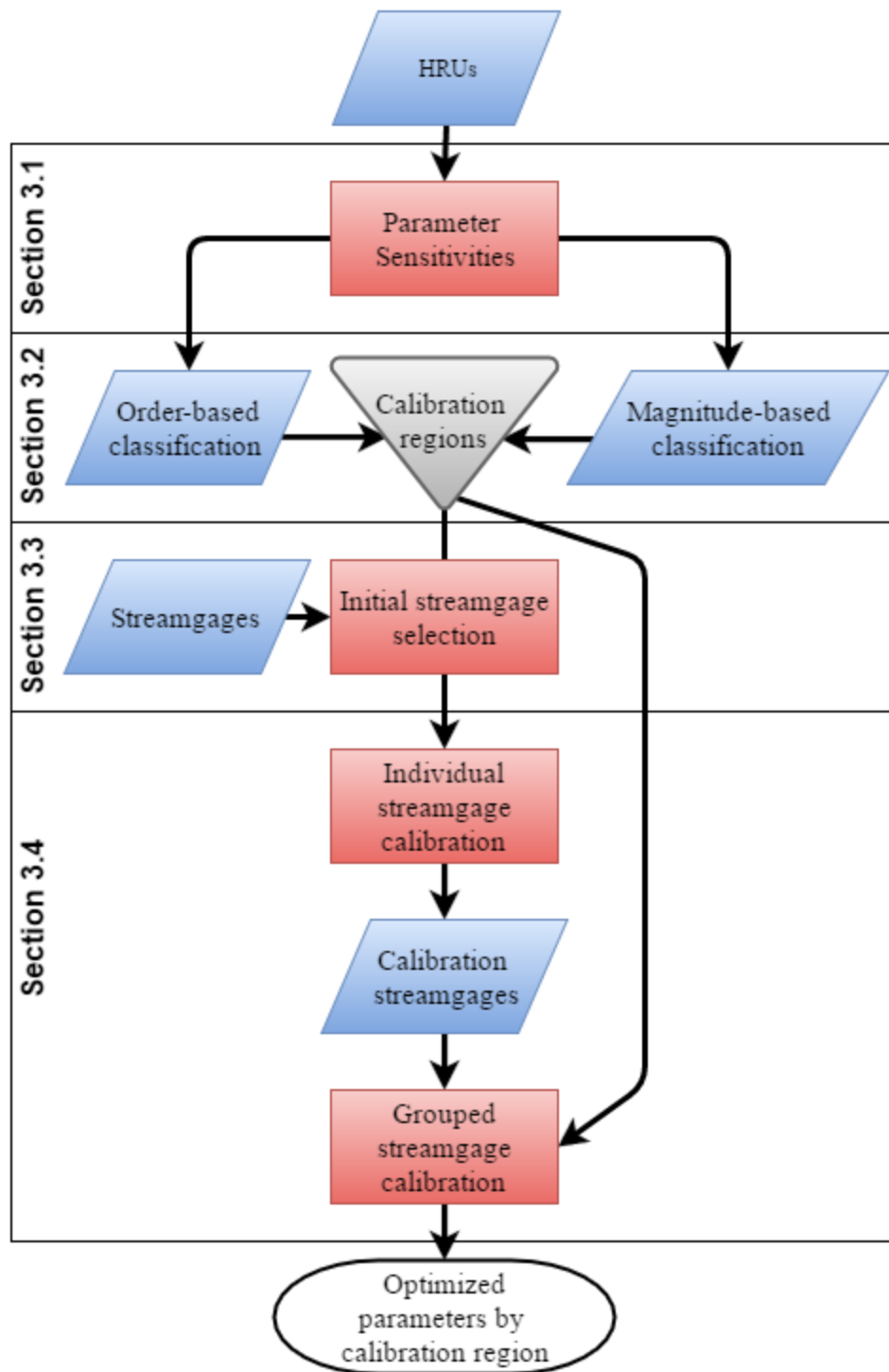
881

882

883

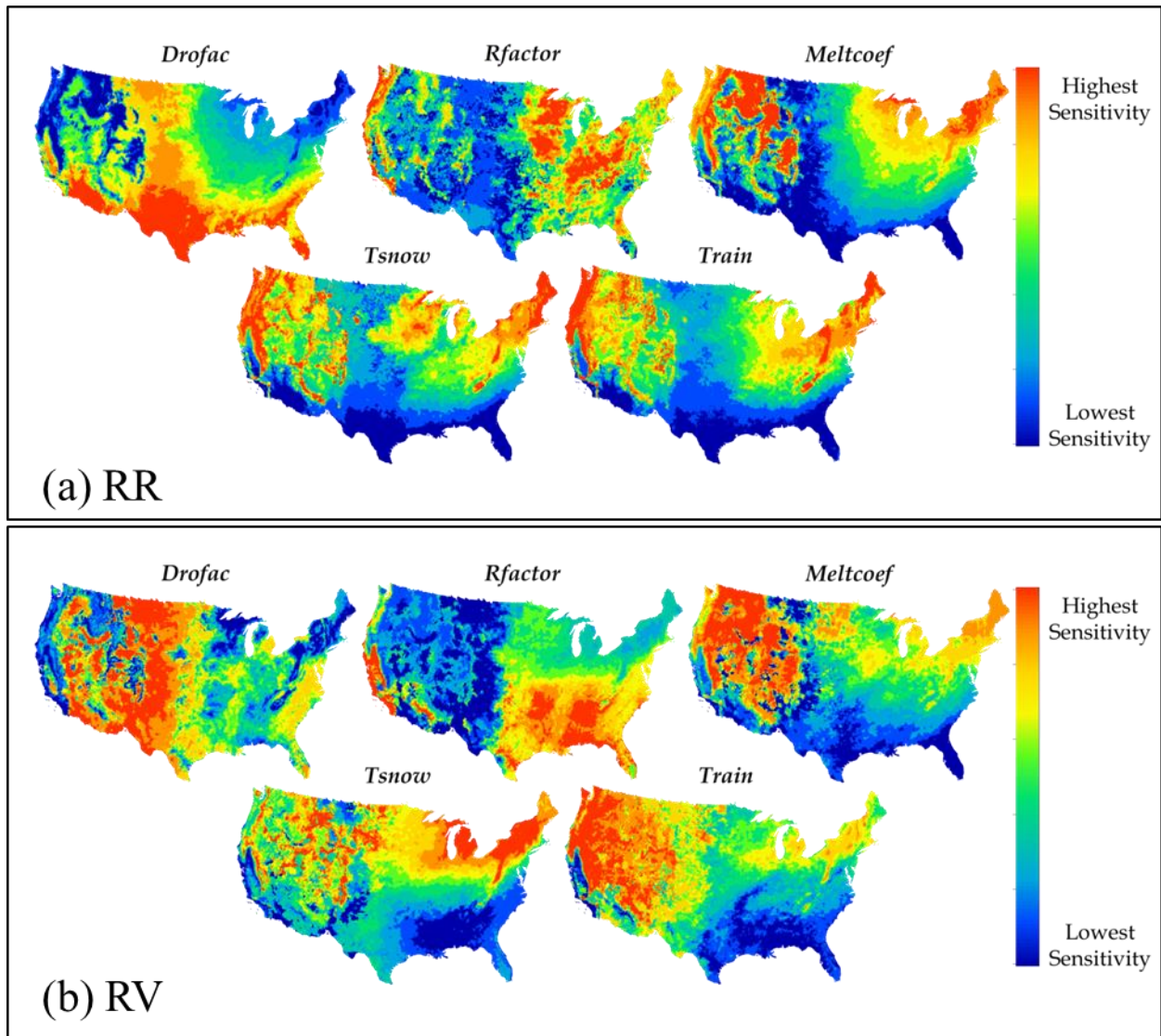
884

885



886

887 *Figure 3. Schematic flowchart of the parameter regionalization procedure described in Section*  
 888 *3: Parameter sensitivities (3.1), Calibration Regions (3.2), Initial Streamgage Selection*  
 889 *(3.3), and Grouped streamgage calibration (3.4).*



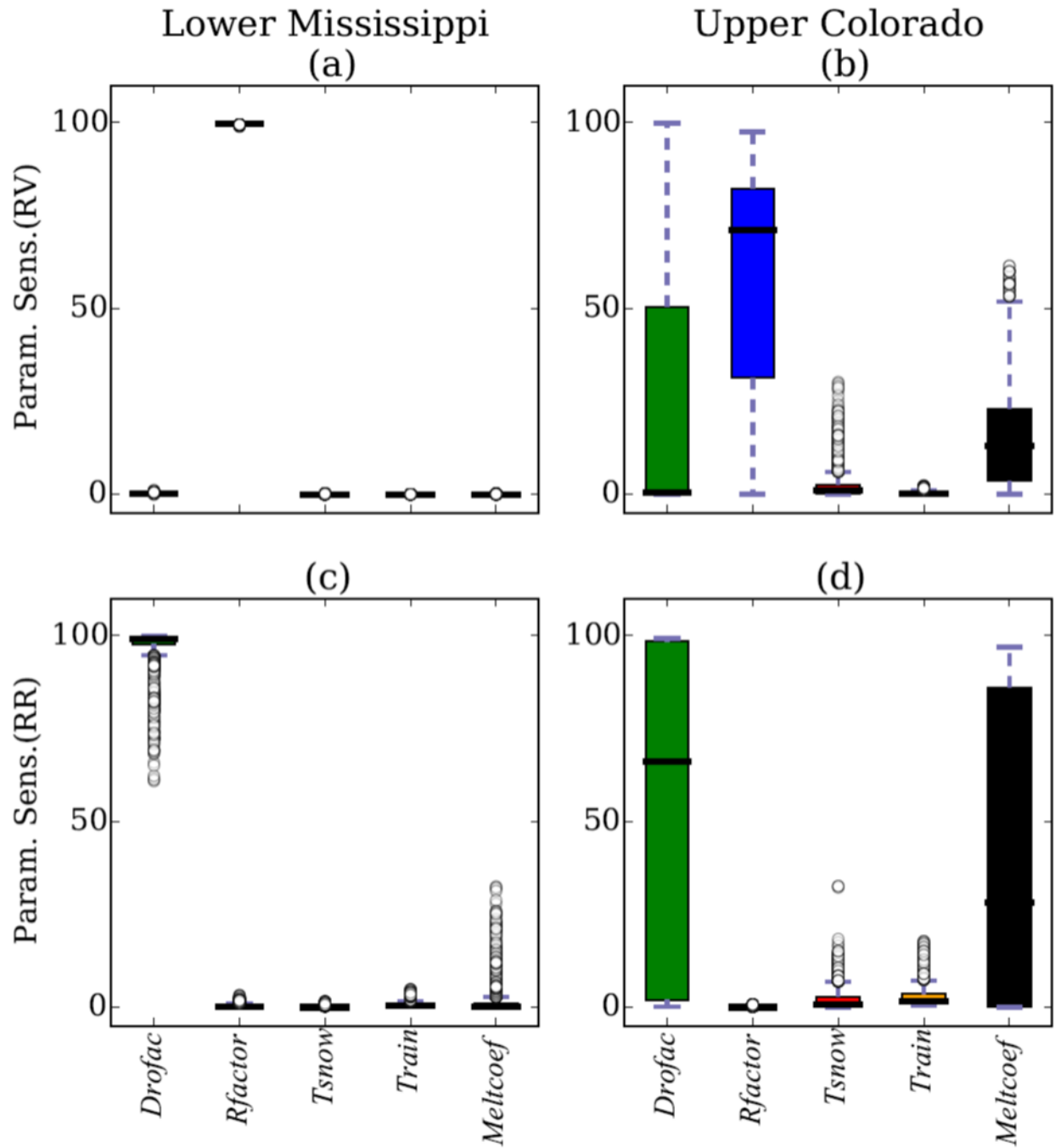
890

891 Figure 4. Relative sensitivity of the (a) Rainfall Ratio (RR) and (b) Runoff Variability (RV)  
 892 indices to Monthly Water Balance Model parameters.

893

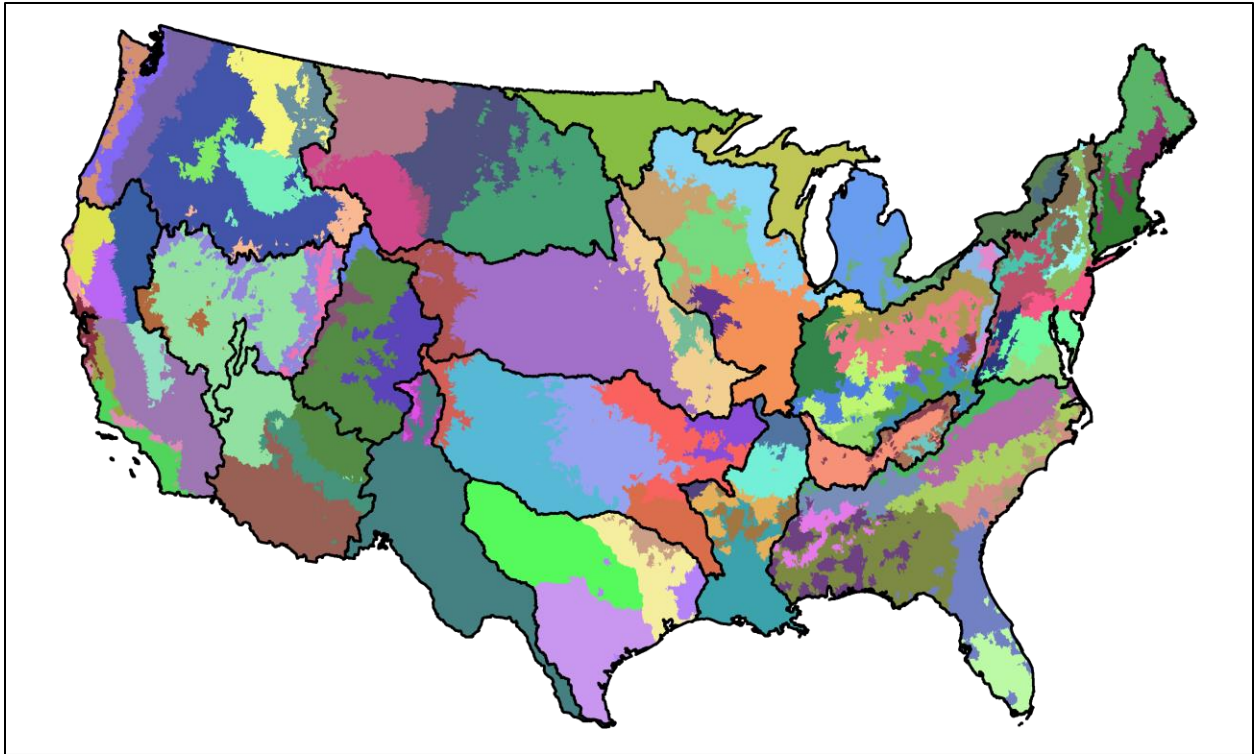
894

895



896  
 897 Figure 5. Parameter sensitivities of Runoff Variability (RV; a and b) and Runoff Ratio (RR; c  
 898 and d) indices for Monthly Water Balance Model parameters in the Lower Mississippi (R08) and  
 899 Upper Colorado (R14).

900



901

902 Figure 6. Final 110 Monthly Water Balance Model calibration regions differentiated by colors.  
903 A subset of streamgages within each calibration region were calibrated in a group-wise fashion  
904 to produce a single optimized parameter set for the entire region (Fig. 3).

905

906

907

908

909

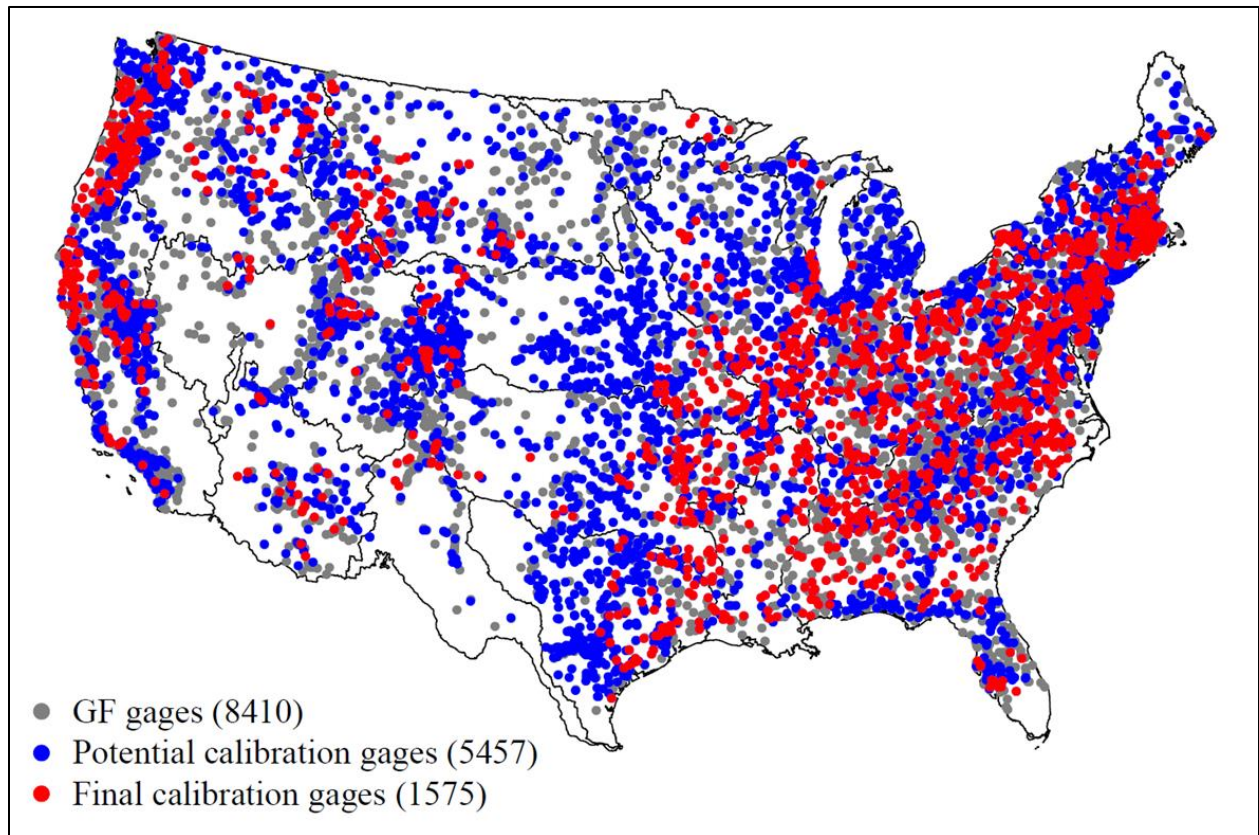
910

911

912



913



914

915 Figure 7. Streamgages tested in the study. GF notes geospatial fabric for national hydrologic  
916 modeling (Viger and Bock, 2014).

917

918

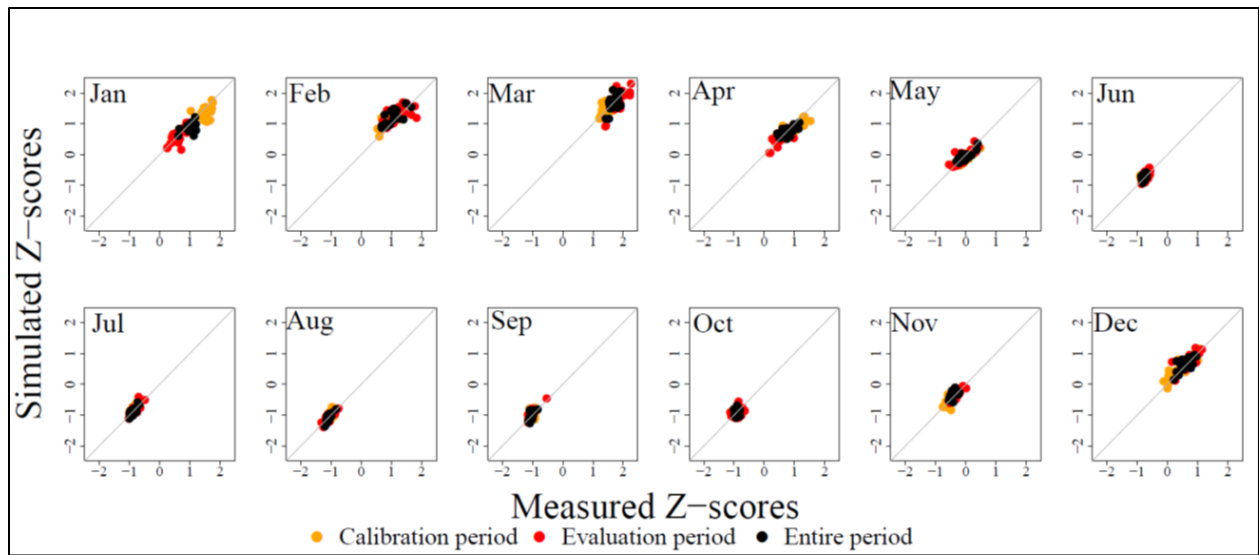
919

920

921

922

923



924

925 Figure 8. Measured versus simulated mean monthly Z-scores for the Tennessee River calibration  
 926 region (see Fig. 9b for location). Orange is calibration, red is evaluation, and black is all years.

927

928

929

930

931

932

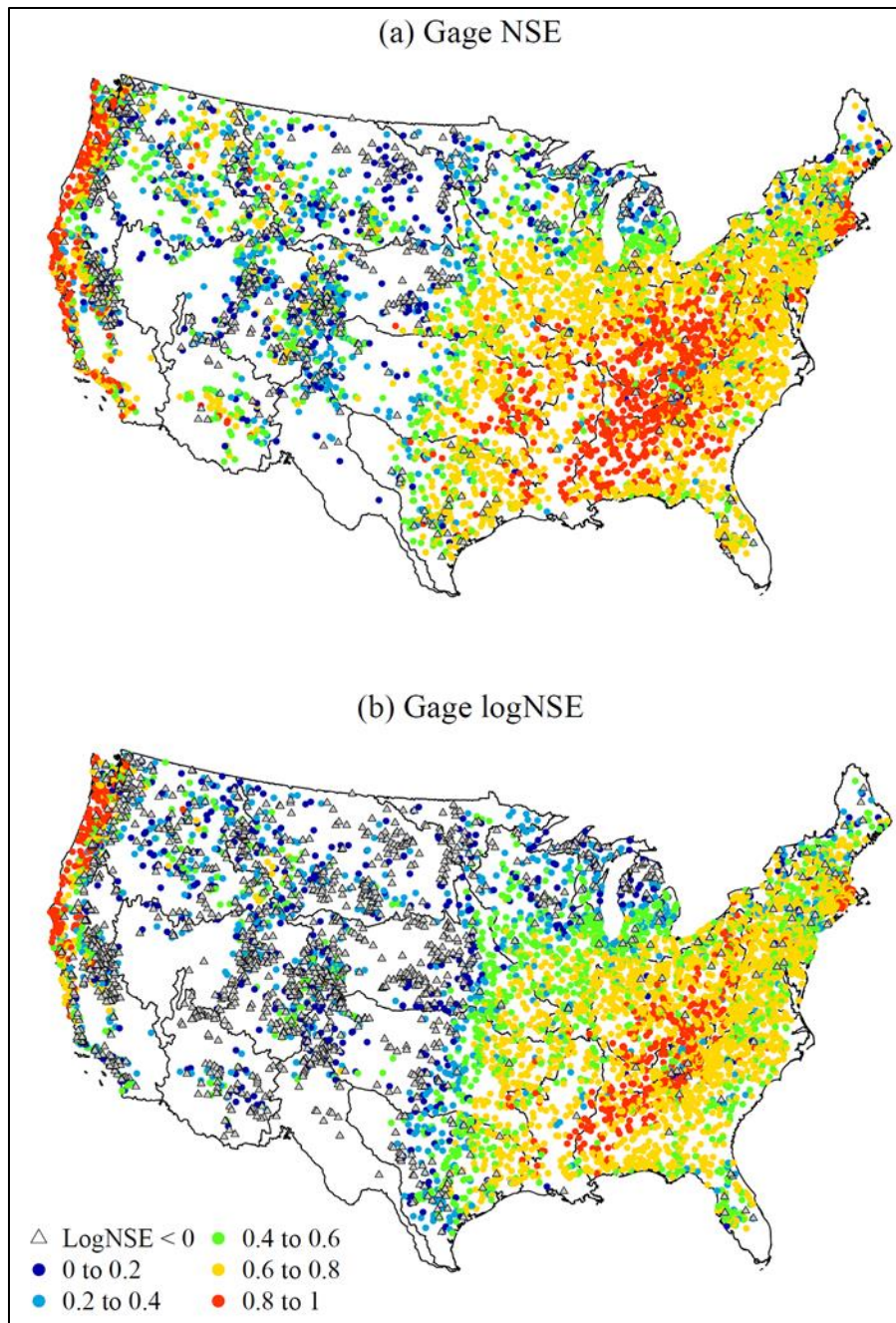
933

934

935

936

937



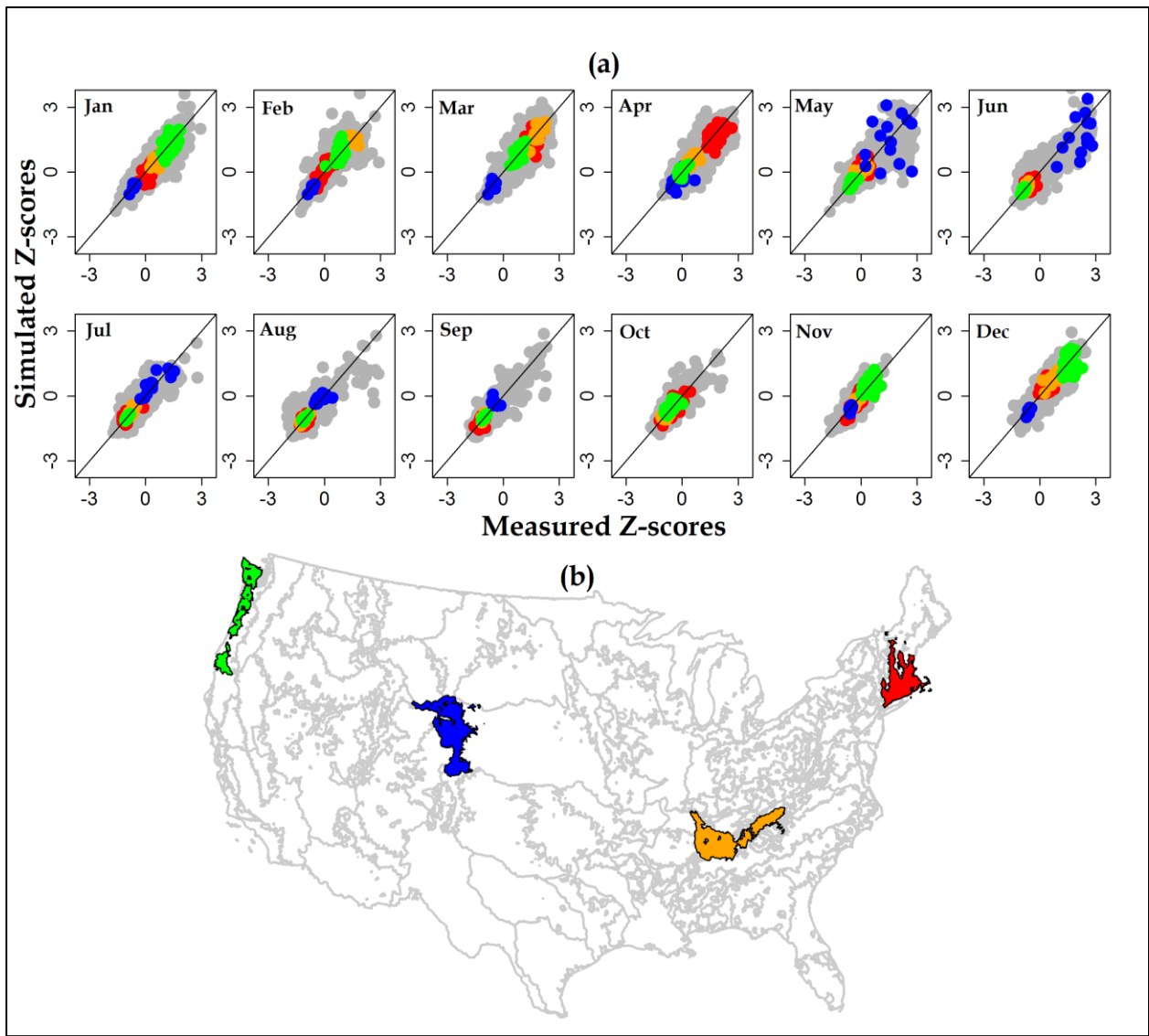
938

939 Figure 9. Individual streamgage calibration results: (a) Nash-Sutcliffe Efficiency (NSE)

940 coefficient and (b) log of the NSE (logNSE).

941

942



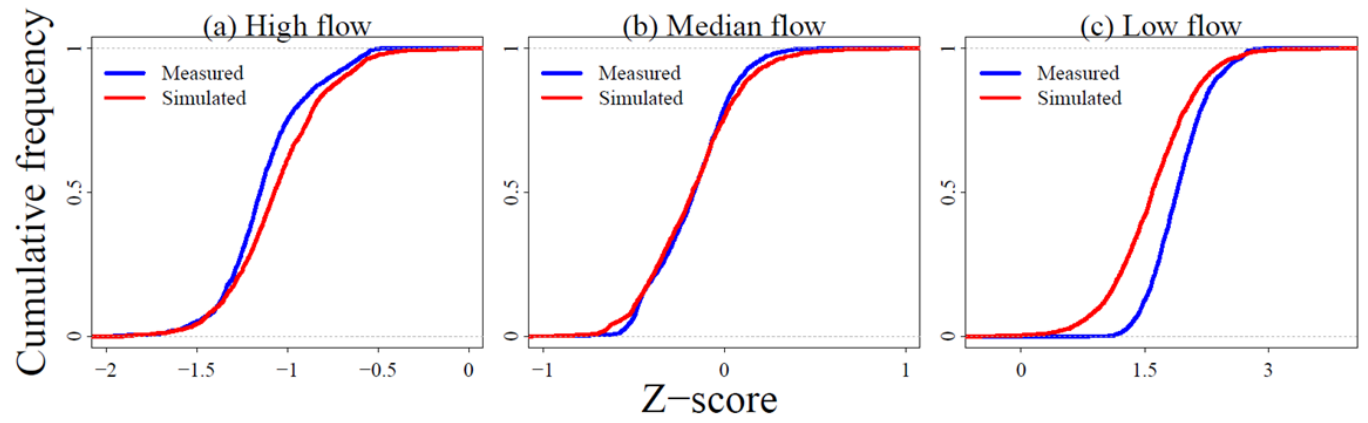
943

944 Figure 10. (a) Measured versus simulated mean monthly Z-scores for runoff at all streamgages  
 945 and (b) location of highlighted streamgages for four calibration regions: New England (67  
 946 streamgages, red); Tennessee River (21 streamgages, orange); Platte Headwaters (15  
 947 streamgages, blue); and Pacific Northwest (33 streamgages, green).

948

949

950



951

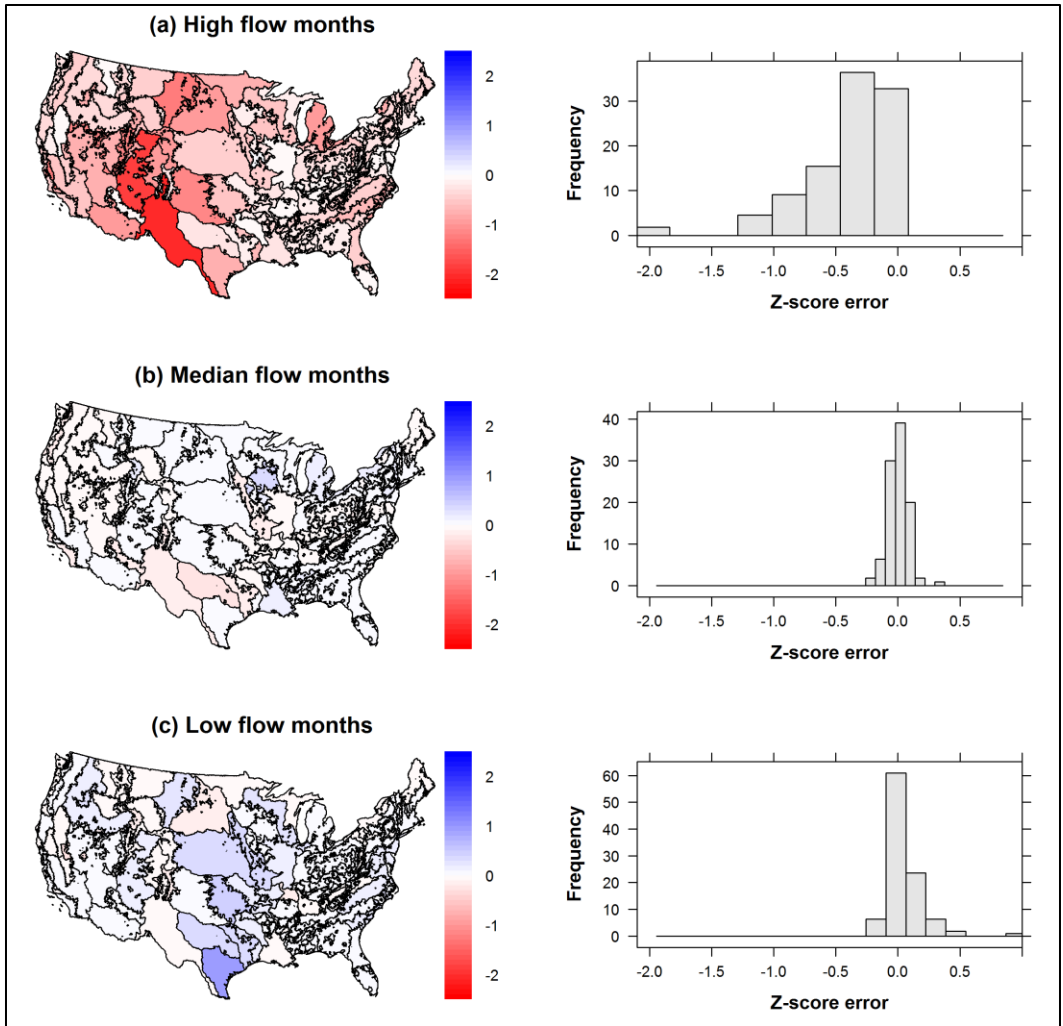
952

Figure 11. Z-score cumulative frequency for (a) highest-, (b) median-, and (c) lowest-flow

953

months.

954



955

956 Figure 12. Z-score error (simulated - measured) for (a) highest-, (b) median-, and (c) lowest-  
 957 flow months.

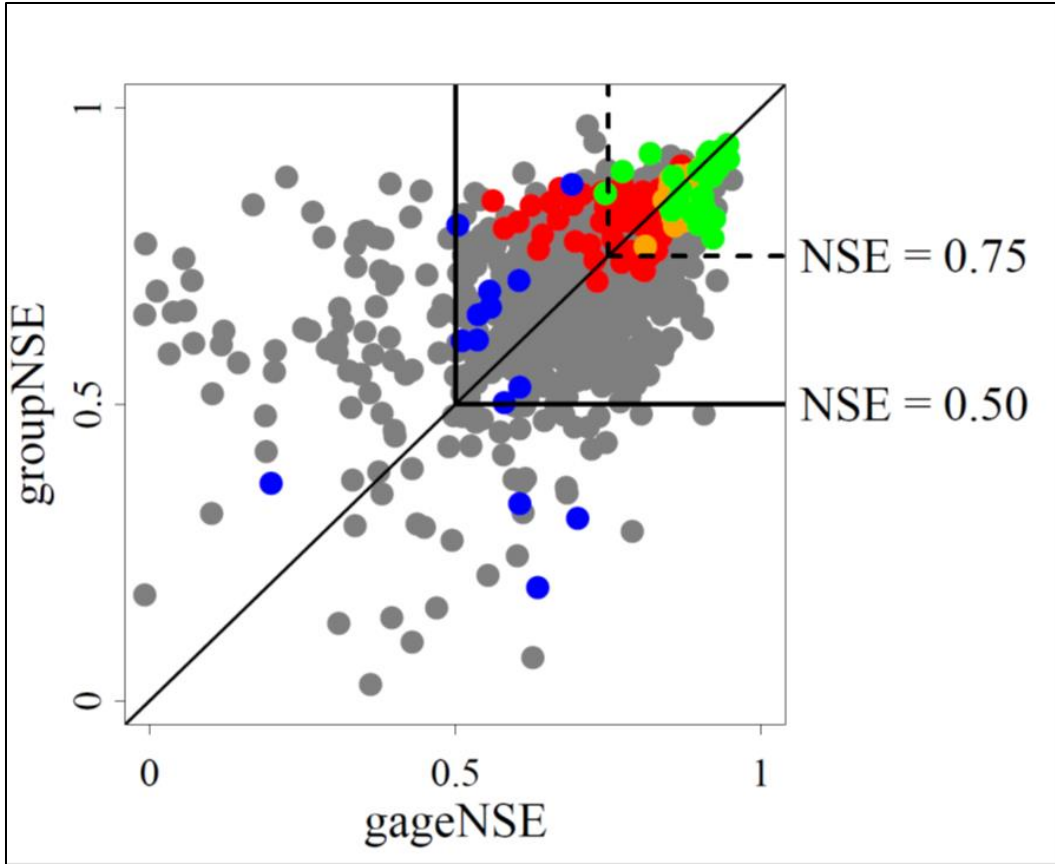
958

959

960

961

962



963

964 Figure 13. Nash Sutcliffe Efficiency from individual (gageNSE) and grouped (groupNSE)  
 965 calibration. Calibration regions in New England (67 streamgages, red); Tennessee River (21  
 966 streamgages, orange); Platte Headwaters (15 streamgages, blue); and Pacific Northwest (33  
 967 streamgages, green) are highlighted (see Fig. 9b for location).

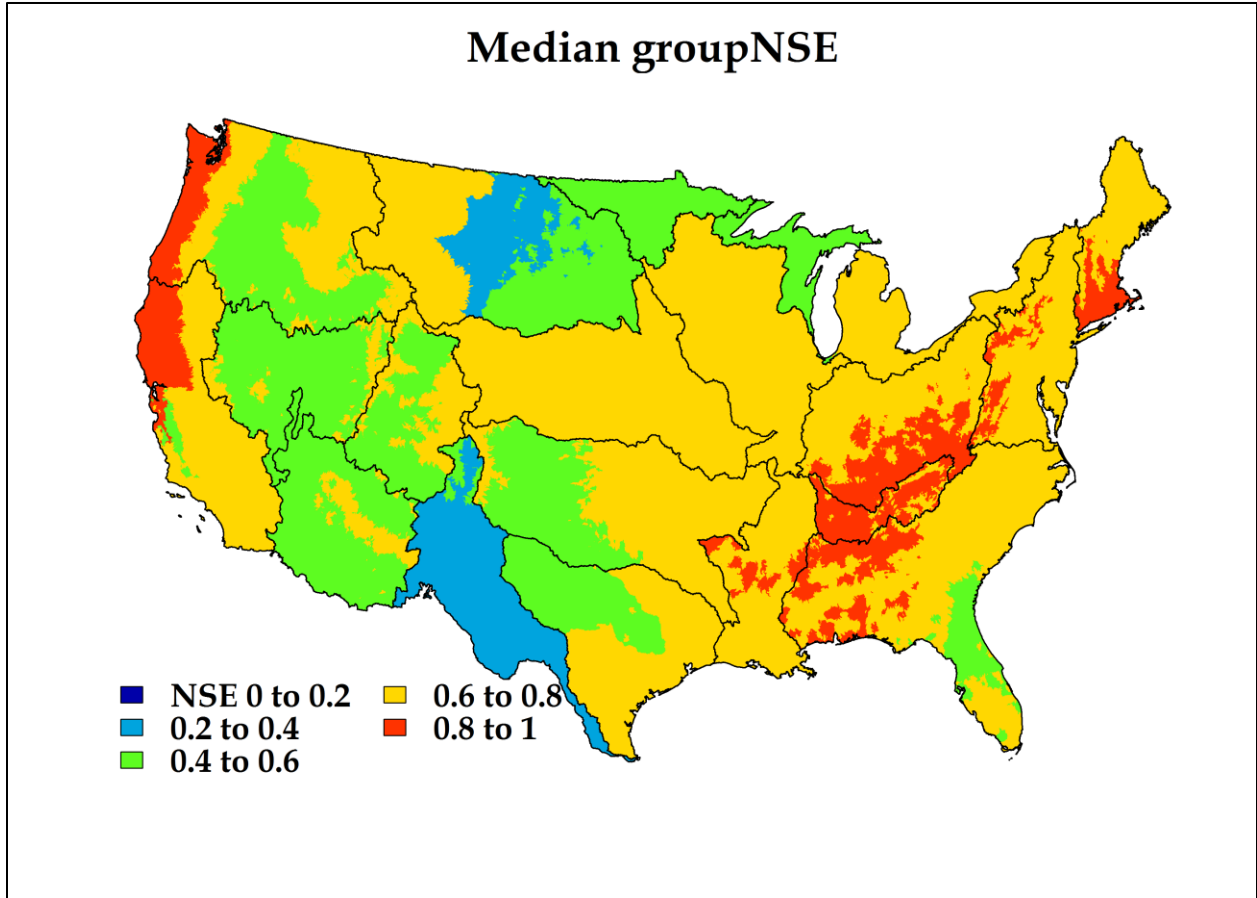
968

969

970

971

972



973

974 Figure 14. Median Nash Sutcliffe Efficiency (NSE) of streamgages used for calibration by  
975 calibration region.

976

977